EFFECT OF PREAGEING AND AGEING PARAMETERS ON THE MICROSTRUCTURE OF 8090 Al Li ALLOY

by

NITIN V. JOSHI

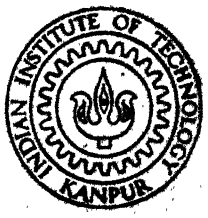

DEPARTMENT OF METALLURGICAL ENGINEERING

INDIAN INSTITUTE OF TECHNOLOGY KANPUR

MAY 1990

EFFECT OF PREAGEING AND AGEING PARAMETERS ON THE MICROSTRUCTURE OF 8090 Al-Li ALLOY

A Thesis Submitted
In Partial Fulfilment of the Requirements
for the Degree of

MASTER OF TECHNOLOGY

by
NITIN V. JOSHI

to the
DEPARTMENT OF METALLURGICAL ENGINEERING

INDIAN INSTITUTE OF TECHNOLOGY KANPUR

MAY, 1990

CERTIFICATE

This is to certify that the dissertation entitled "Effect Of Preageing And Ageing Parameters On The Microstructure Of Al-Li 8090 Alloy" has been carried out by *NITIN V. JOSHI* in the Department Of Metallurgical Engineering, I.I.T., KANPUR in partial fulfillment of the requirements for the Master Of Technology in Metallurgical Engineering under our supervision and has not been submitted elsewhere for a degree.

Dr. T. R. RAMACHANDRAN.
Professor
Department Of Metallurgical Engineering
Indian Institute Of Technology, Kanpur.

MAY, 1990

At Present,
Director,
Jawaharlal Nehru Aluminium Research Development And Design Centre, Nagpur.

Dr. G. S. Murthy.
Programme Co-ordinator,
Department Of Metallurgical Engineering
Indian Institute Of Technology, Kanpur.

Effect Of Preageing And Ageing Parameters On The Microstructure Of 8090 Al-Li Alloy

A B S T R A C T

The reduced density and the increased elastic modulus of Al-Li based alloys compared to conventional aircraft structural aluminium alloys have created intense interest throughout the aerospace industries and associated organisations. AA 8090 (Al-Li-Cu-Mg-Zr) is a newly registered alloy which has the potential of being incorporated into airframes and spacestructures. Microstructural features which influence the mechanical properties of this alloy are : $\delta'(Al_3Li)$ precipitate size and distribution, δ' precipitate-free zone (PFZ), S (Al_2CuMg) precipitate size and distribution and grain boundary precipitates etc.

The present research is focussed on the study of the effect of various preageing and ageing parameters on the microstructure of 8090 alloy. The preageing parameters studied were : natural ageing, low temperature ageing, and slow heating to artificial ageing temperature. Two different ageing temperatures (160^{0}C and 190^{0}C) were studied. Microstructural features of interest, as mentioned above, were investigated by TEM and DSC analyses. Uniform distribution of S phase was observed in a samples; either slowly heated or naturally aged prior to artificial ageing at 190^{0}C.

CONTENTS

List Of Tables

CHAPTER I
INTRODUCTION

In the last two decades, owing to growing energy costs, extensive research and development work is being performed throughout the world in order to reduce structural weight in transport systems by the introduction of new materials. In this connection, Al-Li alloys have aroused extraordinary interest within the aerospace industry and the metallurgical community.

The aircraft manufacturers always search for materials having high strength to weight ratios. Materials with high fracture toughness, corrosion resistance, and fatigue life alongwith low manufacturing and operational costs are the candidate aircraft materials.

The precipitation hardenable aluminium alloys satisfy most of the above requirements, which have made them the dominant structural materials in the aircraft industry for more than half a century. Aluminium - Lithium alloys can be strengthened substantially via precipitation hardening. Compared to conventional alloys, Al-Li alloys have lower density, higher elastic modulus and lower fatigue crack propagation rates. For example, the density of 8090 Al-Li alloy is about 2.56 gm/cc, approximately 10% lower than the conventional aluminium alloys (typical density 2.80 g/cc). Simalarly, the Young's Modulus of 8090 Al-Li alloy is about 81 GPa, compared to about 72 GPa for the conventional aluminium alloys. These property advantages can be exploited for aircraft weight reductions of the order of 15% to 20%. The estimated fuel economy for the projected life of aircraft as a result of the weight reduction is very attractive, and is the chief reason for the considerable efforts which are underway to commercialise Al-Li alloys.

Other materials being developed for similar applications include : Metal Matrix Composites (MMC's), Carbon Fibre Reinforced Polymers (CFRP's), and Laminates. The MMC's in which high strength materials such as SiC, Al_2O_3, B_4C, B etc. are embedded in aluminium alloys typically in the form of particulate, whiskers, or fiber form offer high strength, stiffness, wear resistance, and

elevated temperature stability with 75% improvement in Young's Modulus. The disadvantages are higher production costs, the necessity of redesigning production lines and tooling, and poor ductility (~ 3%). Although CFRP'S offer excellent combination of modulus and density, they are expensive and difficult to fabricate and assemble. Also, their properties are highly anisotropic. Aramid polymer reinforced aluminium laminates (Arall), show a very high strength and larger weight reduction, but question about their durability, binding to metallic structures, and resistance to moisture and delamination need to be answered [1]. In the current situation, all these competing materials seem to have good chances of being used in future aircrafts.

Ingot Metallurgy (I/M), Powder Metallurgy (P/M) [2] and Mechanical Alloying (M.A.) [3] are the three major processing routes which have been used to produce Al-Li alloys. The difficulties in processing are due to the strong reactivity of molten Li [4]. Molten Li reacts readily with oxygen, nitrogen, and moisture etc., and also tends to corrode many crucible materials commonly used. The lower density and melting point of lithium can lead to problems during alloying with aluminium, which might lead to segregation in the cast ingots. Hence, molten Li must be protected by suitable fluxes, or inert atmosphere, and should be mixed carefully with Al so as to avoid direct contact with refractory lining of the aluminium melting furnace. Low carbon stainless steels perform reasonably well for Li melting. Additional problems may be encountered during further processing, e.g. Li loss from surface layers during high temperature exposure.

The precipitation hardening of lithium containing aluminium alloys involves the formation of a metastable, orderded, and coherent δ' (Al_3Li) phase during ageing. The interfacial energy of δ' is very low (~ 25 mJ/m^2) [5] and the low lattice misfit (~ 0.08%) [5], gives lower coherency strains. The major drawback of Al-Li alloys is its lower fracture toughness and poor ductility, which is attributed to factors like planar slip due to the shearable nature of Al_3Li (δ'), δ'- precipitate free zone (PFZ) adjacent to high angle grain boundaries, grain boundary precipitates, and segregation of alkaline impurities such as Na, K, Ca. The planar slip effect can be reduced by achieving a smaller grain size by way of Zr additions [6]. Cu and Mg are added in Al-Li alloys to promote the formation of S phase (Al_2CuMg), which not only contributes to strength but also has effect of homogenising the distribution of slip (by promoting cross-slip [6]). The precipitation of S phase is generally sluggish due to low free vacancy

concentration (because of high Li-Vacancy binding energy), and hence takes place on crystal defects such as dislocations, sub grain-boundaries etc. The kinetics and the distribution of S precipitation can be improved by stretching or natural ageing prior to artificial ageing (by increasing dislocation density and releasing vacancies, respectively).

Extensive research and development efforts are being carried out at Alcan (U.K.), Alcoa (U.S.A.), Cegedur Pechiney (France), Reynolds and Kaiser Aluminium and Allied Chemical Corporation, (U.S.A.). Besides the above companies, it is reported that Martin Marietta Corporation (U.S.A.), Lockheed/NASA (U.S.A.), Royal Aircraft Establishment (U.K.) and Sumitomo corporation (Japan) are also working in the same field.

In U.S.A., Al-Li alloys are being considered for advanced tactical fighter planes, and France, U.K., and Italy are actively pursuing substitution of existing alloys by Al-Li alloys in fighter planes. Boeing commercial airplane company and Douglas aircraft company have scheduled the introduction of Al-Li alloys in early 1990'. Airbus industries will utilise Al-Li alloys in the fuselage, skin panels, stringers, floor beam and seat rails. According to Alcoa, extremely attractive cryogenic properties of Al-Li alloys can be utilised for vessels and tanks in the space vehicles to store liquid H_2 and liquid O_2.

In India, mainly DMRL, Hyderabad and IISc., Bangalore are involved in the development of Al-Li alloys. DMRL has carried out laboratory scale production by Ingot Metallurgy route and plans to cast larger size ingots. The research and development work in IISc. is in association with H.A.L. and A.D.A., Bangalore. NALCO, Bubaneswar, which is at present making available high purity Al (99.8%) required for this work, is expected to play a key role in the large scale production of this alloy [7].

In India, the Al-Li material will be first used for ADA's LCA (Light Combat Aircraft) Programme. The ADA intends to use Al-Li alloys upto 24% of the total material, the major share probably going to the fuselage. Al-Li alloys can also be used for missiles, space vehicles, and other military requirements. It is predicted that country's Al-Li alloy requirement will be around 250 Tons/year from 1995 [7].

The development of a balanced combination of mechanical properties in Al-Li-Cu-Mg-Zr alloys relies on the co-precipitation of δ' and S phases and other microstructural features like the δ'-PFZ. Since stretching prior to ageing may

not be feasible for formed components, alternative means for promoting S precipitation should be studied.

In this investigation, effects of pre-high temperature ageing treatments such as room temperature ageing, low temperature ageing, and slow heating to the artificial ageing temperature are studied in terms of a) the hardening response and b) the microstructure under various conditions. Effect of the artificial ageing temperature is also studied. Such a study is expected to provide better understanding of the response of Al-Li alloys to various thermal treatments, which can be used for optimisation of the microstructure.

CHAPTER II
LITERATURE REVIEW

2.1 : Alloy Design And Development

The low ductility and toughness of binary Al-Li alloys are attributed to (a) strain localisation due to slip coplanarity resulting from shearing of δ' precipitates, and also due to the existance of δ' precipitate free zones (PFZ's) near grain boundaries, and (b) early void initiation at grain boundary particles. In order to improve the ductility of Al-Li alloys, several methods have been suggested. These are 1) increase the lattice misfit between the matrix and δ' [8,9] 2) co-precipitate non-shearable particles [6,10] 3) introduce non-shearable dispersoids [11,12] and 4) reduce grain size [13,14]. The first three methods are aimed at reducing slip coplanarity while the last one is aimed at reducing the slip length and hence the stress concentration at the grain boundaries. Each of these methods is considered in detail below.

1. Alloying additions like scandium, and silver were tried to increase lattice misfit between δ' and matrix. This approach, however, was unsuccessful either due to the low solubility of the alloying elements or their negative contribution towards density, (like Ag and Zn).

2 Co-precipitation of additional non-shearable phases was attempted by additions of Cu and/or Mg. Elements like copper having limited solid solubility, have a great strengthening effect by coprecipitating non-shearable particles with Li. However, the higher copper containing phases promote anodic dissolution at the grain boundaries which is not favourable. Magnesium is a well known solid solution strengthener in Al alloys. Mg reduces solubility of Li in aluminium and promotes the formation of greater volume fraction of δ'. Mg reduces density linearly and improves corrosion resistance and strength in over-aged Al-Li alloys [15]. Al-Li-Mg alloys have shown a great commercial promise, e.g. the Soviet alloy 01420 [14,16,17,18]. When Cu is added to Al-Li-Mg alloys, it is possible to precipitate non-shearable phase S (Al_2CuMg), which increases the strength, homogenises slip, suppresses the $\delta' \rightarrow \delta$ transformation at grain boundaries and decreases the PFZ width [19,20,21]. In Al-Li-Cu-Mg alloys, if the Mg % is not adequate it gives rise to the precipitation of T_1 rather than S phase. S phase is promoted only in alloys

having Mg > 0.7% [22]. Both Cu and Mg strengthen the matrix and/or PFZ either by solid solution strengthening (as is the case with Mg) or by co-precipitation (as is the case with Cu).

3 One method to combat the toughness problem is to add small amounts of an alloying element which would promote the formation of homogeniously distributed dispersoid. Fine dispersoids interact directly with dislocations, dispersing slip and inhibiting the formation of intense slip bands. Also, the dispersoids strengthen PFZ's. Dispersoids must be fine enough to avoid stress concentration at the matrix-dispersoid interface, promoting void nucleation and early crack initiation.

Varying amounts of dispersoid formers such as Mn, Zr, Ti, Co and Y are studied in Al-3% Li alloys [23]. The use of Mn with Fe as an impurity in Al-Li alloys to prevent intense planar slip resulted in predominantly intergranular failure with no necking [24]. Incoherent $MnAl_6$ particles homogenised slip in the matrix, but strain localisation occurred in larger PFZ's in peak aged condition. Coarse $MnAl_6$ at interdendritic boundaries provided an easy fracture path.

As the solid solubility of dispersoid forming element (Zr) is low in Al, it is extremely difficult to add an effective, fine and homogeniously distributed dispersoid in small amounts by a conventional ingot metallurgy. RSP processing is necessary to obtain a complete solid solution. Whilst, If the volume fraction of the dispersoid is low; their strengthening contribution becomes secondary in nature. Ti and Co were added by rapid solidification technique. Annealing around 500°C results in precipitation of Al_3Ti and Co_2Al_9 [23]. The ductility of Al-3%Li was improved from 3.8% to 9.7% and 9.1% due to Ti and Co additions, respectively . It was attributed to delocalisation of slip. Another advantage of Co_2Al_9 is increased high temperature strength. Study on effect of Mo, Nb, W, Fe, Zr, Ni, Ti, and V additions in Al-Li alloys have been reported [25]. As-splatted hardness increased notably. Mo demonstrates outstanding behaviour, both in stability at 540°C and in response to ageing at 160°C. No Al-Mo phases were identified; the interpretation is complicated by inconsistencies concerning the identity of aluminide phases in the Al-Mo binary system.

4 Coarse grain structure do exihibit a low ductility as a result of work hardening and stress concentrations at grain boundaries. Al-Li alloys are no exception. Under commercial development of Al-Li alloys, therefore, control of grain structure via grain refining additions was an immediate task.

Chromium additions were strictly limited since it was proved to be highly ineffective in inhibiting recrystallisation in Al-Li alloys [26]. Whilst, Mn additions form Al_6Mn dispersoid. However, the result was fully recrystallised structure. This was attributed to the dissolution of fine incoherent Al_6Mn during solutionising treatment together with the loss of manganese towards formation of coarse intermetallics like $Al_{12}(FeMn)_3Si$, Al_9MnSi etc. [27] during solidification. Consequently, Mn additions received little attention in the later stages of commercial development of Al-Li alloys.

Recently additions of the group 4A transition metals (Ti, Zr, & Hf) was studied [28]. These lead to duplex precipitation hardening behaviour throgh the formation of $Al_3(TM,Li)$ (TM = Transition element), which act as strengthening precipitates (due to its composite form) and also as a grain refiner. The improvement in mechanical properties by grain refining can be estimated by Hall-Petch equation. As strength is inversely proportional to grain size. Slip dispersion, reduced slip length and PFZ strengthening by β' $Al_3(TM)$ are primarily responsible for the improvment in mechanical properties.

Zirconium appears to have two potent beneficial effects in the Al-Li system. First, alloys which contain Zr tend to have a finer grain structure than those containing either Mn or Cr. Second, the Al_3Zr precipitates retard recrystallization by impinging on grain boundaries and thereby inhibiting their migration. In addition, the Al_3Zr particles also contribute some dispersion strengthening to the alloy [29,30]. The non-shearable nature of the Al_3Zr phase is expected to preclude the intense slip localisation of binary alloys.

Based on the above concepts a five-component composition registered as AA 8090 was developed by ALCAN (U.K.), Pechiney (France), and ALCOA.

Designation	Trade name	Composition				Others
		Li	Cu	Mg	Zr	
8090	DTD XXXA LITAL A CP 271	2.20- 2.70	1.00- 1.60	0.60- 1.30	0.04- 0.16	0.00-0.20 Si 0.00-0.30 Fe 0.00-0.10 Cr 0.00-0.15 Ti 0.00-0.25 Zn 0.00-0.10 Mn

2.2 : Phase Eqilibria And Transformations

2.2.1 : Phase Diagram Of Binary Al-Li System

The portion of the binary Al-Li phase diagram is shown in Fig. 1 [31]. The principle phases of interest in the binary alloys are the equilibrium α (Al-Li solid solution), equilibrium δ (AlLi), and metastable δ' (Al_3Li). Metastable solvus lines corresponding to the δ' phase are shown in Fig. 2 [32]. The maximum solid solubility of lithium in aluminium has been found by microscopic methods to be 4.2 wt % at the eutectic temperature (about 600^{o}C) which controls the maximum allowable Li content in precipitational hardenable alloys [33]. It is clear from the δ' solvus lines shown in the Fig. 2 [32] that only the alloys with Li content exceeding 1.7 wt % can give rise to the metastable δ' phase upon age hardening.

The eqilibrium δ phase has cubic (NaTl) crystal structure. The metastable phase δ' has an $L1_2$ type superlattice structure and is fully coherent with the matrix (lattice misfit ~ 0.08 %) and has an interfacial energy ~ 25 mJ/m2 [34]. Various values of lattice misfit parameter and interfacial energies have been reported in the literature and are summarised by Williams [35]. δ' is spherical in shape possessing a cube-cube orientation with the matrix. The sloping metastable solvus line towards the δ' end indicates that non-stoichiometric compositions may occur in δ', particularly at higher ageing temperature. The diagram calculated by Sigli et al. Fig. 1 [31] predicts a miscibility gap, which is metastable with respect to both the α-δ and α-δ' equilibria : it therefore lies within the α+δ' phase field. The practical consequence of this will be considered in the following section on transformations.

Certain amount of uncertainties exist regarding the various solvus lines in Al-Li phase diagram [35], the determination of which by conventional microanalytical techniques proves to be very difficult due to the low atomic number of lithium.

2.2.2 : Phase Eqilibria In Multicomponent Al-Li Based Systems

Although limited amount of imformation is available on the various ternary systems involving two of the alloying elements (Cu and Mg), no such information is available for quaternary or the more complex commercial compositions. The phase diagram of the Al-Li-Cu-Mg system has not been determined. The commercial production of these complex heat-treatable alloys requires a knowledge of the solubility limits of the major alloying elements so as to decide the homogenising

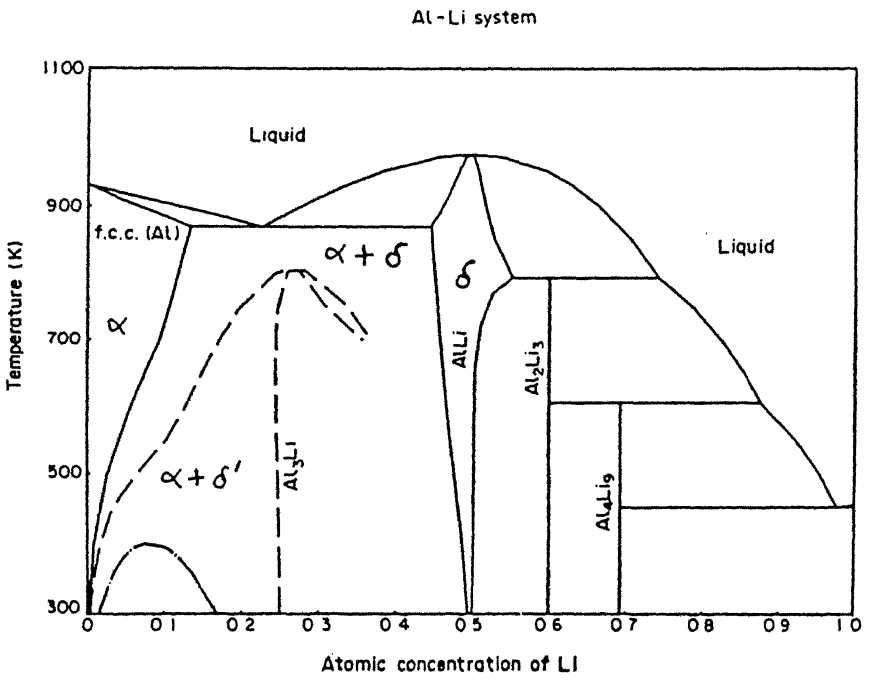

Fig. 1 Calculated Al-Li phase diagram, dashed lines are metastable ' (solid solution) - δ' (Al_3Li) two phase boundary, and dashed-dot line is metastable miscibility gap for supersaturated solution.

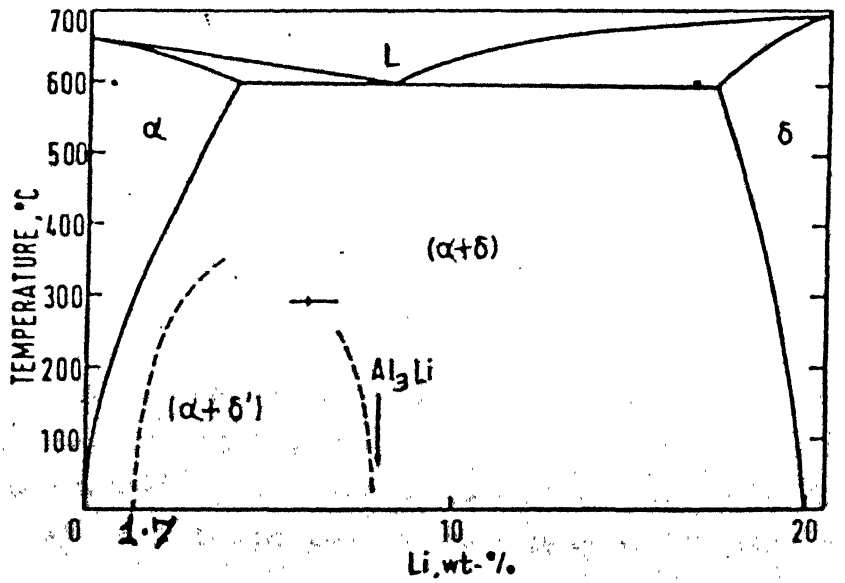

and solution heat treatment temperatures. Recently a study on the determination of solvus and solidus temperatures of commercially relevant compositions has been reported [36]. The compositions covered the range 2.0 to 2.7 % Li, 0.5 to 2.8 % Cu, and 0 to 1.5 % Mg, refer Table I [36]. The alloy no. 6 is equivalent to 8090 composition. This table lists the apparent melting and solvus temperatures based on metallographic evaluation. All the alloys except #18 showed distinct α -- α + 1 phase equilibria, so the melting points can be considered to be solidus temperatures. Alloy 18 was supersaturated and did not exhibit a single phase region. For purposes of generating solvus and solidus isotherms, the data were subjected to a statistical multiple regression analysis [37]. The mathematical representation is as

T (solvus) = 284 + 67.0 (pct Li) + 34.6 (pct Cu) + 36.5 (pct Mg) eq. [1]

T (solidus) = 730 - 24.5 (pct Li) + 33.2 (pct Cu) - 49.0 (pct Mg) + 10.0 (pct Mg)^2 eq. [2]

Zr addition in quaternary Al-Li alloys forms metastable, coherent, $L1_2$ ordered β' precipitate (Al_3Zr or $Al_3(Zr,Li)$). The lattice parameter of β' is close to that of aluminium. The phases in heat treated Al-Li-Cu-Mg-Zr alloys are shown in Table II [38]. The orientation relationship of T_1 and S with the matrix appears to be the same as that found in the ternary alloys.

2.2.3 : Phase Transformations

δ' (Al_3Li) Phase

Quenching the Al-Li alloys from solutionising temperature, an alloy enters the α (solid solution) + δ' phase field and decomposes to produce lithium rich Guinier-Preston (G.P.) zones. This reaction could involve classical nucleation and growth or spinodal decomposition within the α and δ' spinodes. Evidence for such a transition has been adduced from the interpretation of DSC data [35]. The first study to propose the existance of precursor phase to the δ' was by Nozato et al. [39]. Since then, several studies using thermal analyses [40,41], resistivity [42], and SAXS [43,44] have all shown similar results. The results by Papazian et al. [41] are in excellent agreement with the calculations of the Sigli et al. [31].

The alternative explanation for the thermal analysis data is that the thermal anomalies are manifestations of the fine δ' that becomes sub-critical in size as ageing proceeds and matrix supersaturation decreases [45]. This point was considered at some length by Mukhopadhyay et al. [40] who concluded that the

Table I Chemical compositions, melting points, and solvus temperatures of Al-Li-Cu-(Mg) alloys.

Alloy Number	Pct by Wt Li	Cu	Mg	Melting Temp. (°C)	Solvus Temp. (°C)
1	1.96	2.68	0.00	595	500
2	2.23	2.76	0.00	585	525
3	2.40	2.66	0.00	580	540
4	2.67	2.83	0.00	570	560
5	2.58	2.80	0.18	565	560
6	2.47	1.22	0.67	600	515
7	2.53	2.13	0.67	565	555
8	2.25	2.06	0.47	585	530
9	1.98	1.89	1.47	570	540
10	2.13	2.38	0.48	575	530
11	2.15	2.08	1.03	570	540
12	2.37	0.53	1.30	605	505
13	2.63	1.73	0.92	575	545
14	2.18	1.91	1.49	560	545
15	2.39	1.29	0.76	595	515
16	2.23	2.52	0.99	555	550
17	2.48	1.86	0.84	570	545
18	2.50	2.59	1.06	555	insoluble
19	1.99	2.70	0.47	570	530
20	2.28	1.72	0.89	585	535
21	2.35	2.12	0.72	570	545
22	2.38	2.03	0.92	560	550
23	2.69	1.27	0.79	595	540
24	2.47	2.36	0.69	565	560

Table II Phases in heat treated Al-Li-Cu-Mg-Zr alloys

Phase	Composition	Crystal Sructure	Stability	Morphology
δ'	Al_3Li	$L1_2$	Metastable	Spherical
δ	AlLi	Cubic	Stable	Equiaxed
T_1	Al_2LiCu	Hexagonal	Stable	Plate
T_2	Al_6Li_3Cu	Icosahedral	Stable	Plate
S'	Al_2CuMg	Orthorhombic	Metastable	Plate
S	Al_2CuMg	Orthorhombic	Stable	Equiaxed
β'	Al_3Zr	$L1_2$ (Cubic)	Metastable	Spherical

evidence was firmly in favour of G.P. zone model. A problem that remains is that the G.P. zones have never been observed directly in TEM or the FIM. TEM diffraction contrast images will never reveal the G.P. zones because the inevitable presence of strong δ' contrast will mask the small strain contrast from the G.P. zones. Therefore, it is necessary to use a technique such as high resolution phase contrast imaging which should easily distinguish G.P. zones and δ'. Alternative interpretations invoke very fine δ' produced on quenching the formation of which would, of course, inhibit G.P. zone precipitation (spinodal decomposition).

The study by Janos et al. [46] show that there is no relavant structural difference between the precipitates formed at room temperature and those formed in the temperature range 130°C to 200°C. The only difference is in the size and in the quality of the particle/matrix interface and a probably higher defect concentration in the small particles. These differences, however, in the author's opinion do not require the introduction of a G.P. zone phase which would be physically different from the δ' phase. Therfore, it is the author's belief that the decomposition of the supersaturared solid solution in Al-Li alloys of compositions between about 5 and 14 at% in the temperature range from room temperature to 200°C takes place by the formation of metastable δ' precipitates and there is no physical reason to postulate another level of metastability, i.e. the existence of G.P. zones in this system.

The interesting results by the same author [46] has shown that in artificially aged (at 160°C and 200°C) Al-Li alloys further nucleation of δ' takes place during room temperature storage. The reason for this post-ageing phenomenon is : significantly different solubility of Li in Al at 160°C or 200°C and at room temperature, respectively. After artificial ageing, when the sample is transfered to room temperature, the solid solution becomes supersaturated again and consequently further precipitation sets in as confirmed by HREM. TEM and HREM micrographs reveal a bimodal distribution of δ' precipitates with considerably different mean particle sizes. This precipitation taking place by the formation of new particles instead of further growth of the already existing large δ' particles indicates that no significant nucleation difficulty is involved in the precipitation. This is consistent with the lower particle/matrix interface energy and misfit strain energy in the case of the fully coherent δ' precipitates.

δ' (Al_3Li) nucleates preferentially at β'(Al_3Zr)-α (matrix) interface. There is also evidence of Mg in δ' in Al-Li-Mg alloys [47]. Magnesium increases the lattice

parameters of both δ' and matrix. The lattice expansion exhibited by the δ' particles indicate the presence of Mg [47]. When Mg level exceeds 2% or ageing treatments are prolonged (e.g. Al_2MgLi forms).

T_1 and S phase

Within the 8090 composition specification, changing the Mg content of the alloy changes the relative proportions of S (Al_2CuMg) and T_1 (Al_2CuLi) phases. When Cu : Mg proportion is more than 2, T_1 predominates [22]. But, when Mg content is increased to the level of Cu : Mg proportion of about 2, T_1 is replaced by S phase. Magnesium content of atleast 0.7% is necessary for S precipitation [22]. Both T_1 and S precipitation is encouraged by deformation prior to ageing; precipitation is preferably at the dislocations and sub-grain boundary region.

An alternate method for widespread precipitation of S phase involves increasing the amount of Cu and Mg supersaturation in the alloy such as the situation in the 8091 alloy. The strong lithium/vacancy interaction slows the kinetics of precipitation of S phase in more dilute 8090 alloy. Therefore homogeneous 'S' is not obtained by usual ageing practice. Low temperature ageing or natural ageing results in the growth of δ' and the simultaneous liberation of bound vacancies thereby aiding homogeneous precipitation of S phase [48].

β' (Al_3Zr) Phase

Three possible β' nucleation mechanisms were suggested : homogeneous nucleation, preferred nucleation at T phase, and nucleation which leads to discontinuous precipitation [49]. But in general, during homogenisation high density of β' particles is formed. It has been deduced that it forms via homogeneous nucleation, since the preferred nucleation and discontinuous nucleation did not bring about fine dispersion of β'. It forms in the early stages of homogenising (around 500^0C). β' is a metastable, sherical and ordered phase. It has $L1_2$ type structure. Dispersions of these particles are very stable at the solution treatment temperatures due to low diffusion rate of Zr in Al [50]. Diffusivity of Zr in Al has been estimated to be about 10^{-11} cm^2/sec. The Al_3Zr dispersoids acts as a heterogeneous nucleation sites for δ' during ageing. This results in a duplex δ' in the matrix (Bull's eye or Do-nut structure) [47,51].

δ (AlLi) Phase

The mechanism of the formation of δ phase is still unknown. Niskanen et al. [15] have suggested that the formation of δ on grain boundaries is the result of

preferential coarsening of δ'. The boundaries provide the energy required to overcome the interfacial energy barrier of the $\delta' \rightarrow \delta$ transformation. However, Venables et al. [52] presented diffraction evidence for the nucleation of δ at α (matrix)/δ' interface. To support this argument it was proposed that δ must form as a coherent precipitate and transform to an incoherent precipitate later on its development. Given the enormous difference in lattice parameters (about 50%) between δ and δ', and the difference in crystal structure, this mechanism must be considered doubtful [35]. Williams et al. [53] suggested that the small amount of lattice strain generated by coherent δ' phase is not sufficient to justify its possible use as a nucleation site for δ. Williams [53] hence suggested that δ nucleates heterogeneously on the grain boundary and within the matrix independent of δ'.

T_2 Phase

The T_2-$Al_6Cu(Li,Mg)_3$ compound has been reported to precipitate during casting. It is undissolvable during homogenising and subsequent processing of the alloy. T_2 also forms along the grain boundaries in peak-ageing and over ageing of Al-Li-Mg based alloys [54,6]. Its formation during ageing with δ at grain boundaries, leads to weakening of grain boundaries. It aids δ' PFZ formation adjacent to grain boundary. It has raised a considerable interest since the discovery of its quasi-crystalline structure [55]. The homogeneous nucleation and coarsening of T_2 is observed in 2091 (Al-Li-Cu-Mg-Zr) alloy [56]. Precipitation of T_2 inhibits the benefit of S nucleation by stretching before ageing to the T 651 or T 8 tempers [57].

Crystallographic details of the phases occurring in Al-Li-Cu-Mg-Zr alloys are summarised in Table III [58].

..... Continued on next page

Table III Crystallographic details of phases occurring in Al-Li-Cu-Mg-Zr alloys

Phase	Crystal structure*	Orientation relationship	Remarks
AlLi (δ)	Cubic ($NaTl$) $a = 0.638$	$(100)_p // (110)_{Al}$ $(011)_p // (\bar{1}11)_{Al}$ $(0\bar{1}1)_p // (1\bar{1}2)_{Al}$ Habit plane $(\bar{1}\bar{1}1)$	Equilibrium phase in the form of plates; addition of Cu or Mg does not affect the lattice parameter
Al_3Li (δ')	Cubic ($L1_2$) $a = 0.401$	Cube-cube	Metastable, coherent and ordered phase; spherical shape; lattice parameter varies slightly with Cu or Mg addition
Al_2CuLi (T_1)	Hexagonal, $a = 0.4965$ $c = 0.9345$	$[11\bar{2}0]_p // [2\bar{1}\bar{1}]_{Al}$ $(0001)_p // (111)_{Al}$ $(10\bar{1}0)_p // (1\bar{1}0)_{Al}$ Habit plane (111)	Partly coherent; coprecipitates with δ' for low Cu/Li ratio (2.5Cu : 2Li) at all temperatures; above 170 C for medium Cu:Li ratio (3·5Cu : 1·5Li); for high Cu:Li ratio (e.g. alloy 2020) precipitation sequence follows that in Al-Cu system
Al_6CuLi_3 (T_2)	Cubic, $a = 1.3914$		Displays icosahedral symmetry
$Al_{15}Cu_8Li_2$ (T_B)	Cubic (CaF_2) $a = 0.583$	$(100)_p // (110)_{Al}$ $(001)_p // (001)_{Al}$	
T''	Tetragonal $a = 0.575$ $c = 0.608$	$(001)_p // (001)_{Al}$ $(100)_p // (110)_{Al}$ $(010)_p // (1\bar{1}0)_{Al}$	Atomic ratio of Cu to Al is found to be in the range 0.5 to 1·0
Al_2CuMg (S')	Orthorhombic $a = 0.404$ $b = 0.925$ $c = 0.718$	$(100)_p // (100)_{Al}$ $(010)_p // (021)_{Al}$ $(001)_p // (012)_{Al}$	Semi-coherent; rods grow along $\langle 110 \rangle_{Al}$ which widen forming laths in $\{210\}_{Al}$
Al_2CuMg (S)	Orthorhombic $a = 0.400$ $b = 0.923$ $c = 0.714$	Similar to S'	Forms by coherency loss of S' or by heterogeneous nucleation on grain boundaries; incoherent equilibrium phase
Al_2MgLi	Cubic $a \simeq 2.00$	$(\bar{1}10)_p // (\bar{1}10)_{Al}$ $(110)_p // (111)_{Al}$	Growth direction $\langle 110 \rangle_{Al}$
AlLiSi	Cubic $a \sim 0.594$		
Al_3Zr	Cubic ($L1_2$) $a = 0.405$	Cube-cube	Spherical, coherent and ordered dispersoid particles found in zirconium-containing alloys

2.2.4 : DSC STUDIES

DSC is a useful technique to study the precipitation process. A thorough understanding of the energetics and kinetics of precipitation and dissolution of phases is possible. The DSC technique detects the heat flux into or out of the sample, caused by the imposed temperature programme. The output of DSC is generally presented in mw against temperature or time. The formation of precipitating phases is an exothermic reaction whilst their dissolution is an endothermic reaction. Mukhopadhyay et al. [40] have used DSC measurements to investigate the role of Zr additions to the binary Al-Li system and quaternary alloy (8090). The DSC thermograms for Al-Li, Al-Li-Zr, Al-Cu-Mg, Al-Li-Cu-Mg are shown in Figs. 3 - 6 [40] respectively. The explanation for the abbreviation A.Q., N.A., and A.A. is provided in Fig. 3.

The as quenched material of Al-Li alloy shows exothermic peak (A) at the starting and this behaviour is terminated by the endothermic reaction at 130^{0}C (B). Peak (A) is attributed to Al-Li G.P. zone formation, whereas endotherm (B) has previously been attributed to fine δ' dissolution [59] or G.P. zone dissolution [39,41]. But the work by Baumann [60] and Papazian et al. [41] showed that the small δ' oberved at room temperature is stable against reversion to much higher temperature (~ 170^{0}C for 2.5 wt% Li alloy). This view is reinforced by the observation of the 130^{0}C endotherm in natural aged samples. Therefore, it is concluded that there is indeed a second metastable precipitate phase present additional to δ'. This may well be in the form of G.P. zones, which are not imaged in TEM because of the presence of the very fine δ' which dominates the microstructure. The results imply that δ' and G.P. zones grow competitively at room temperature storage and natural ageing enlarges the 130^{0}C endotherm peak and is observed to produce larger δ' particles. The absence of this 130^{0}C peak in artificially aged samples implies that the G.P. zones have been completely replaced by δ'. The 170^{0}C exotherm is attributed to δ' precipitation and δ' dissolution peak at D_2. Peak D_2 is well above δ' solvus temperature, and is possibly truncated at high temperature, by the exothermic δ(AlLi) formation reaction. In the author's opinion, the explanation for broadening of D_2 (D_1 and D_2) based on dissolution of different diameter δ' is misleading. The broadening of D_2 during ageing (artificial or natural) is related to the concentration of Li in solution compared with the position of δ' solvus. In as-quenched materials a lower volume fraction of δ' is present on heating in the DSC above 185^{0}C than in either of the other two cases.

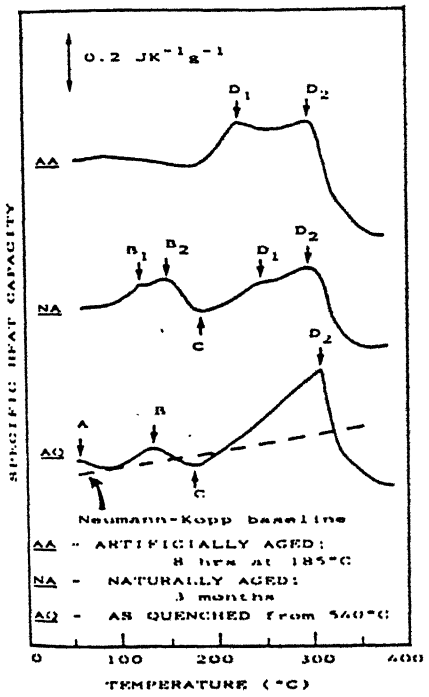

Fig. 3 Specific heat capacity curves for Al-Li alloy.

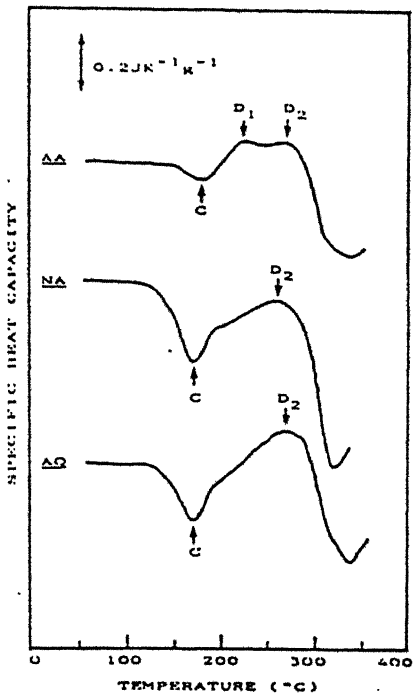

Fig. 4 Specific heat capacity curves for Al-Li-Zr alloy.

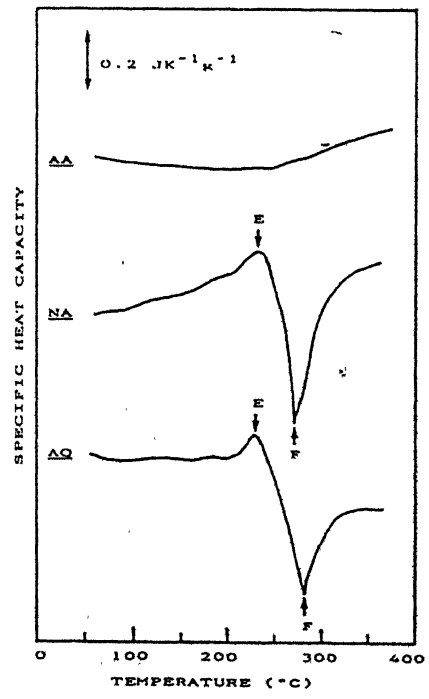

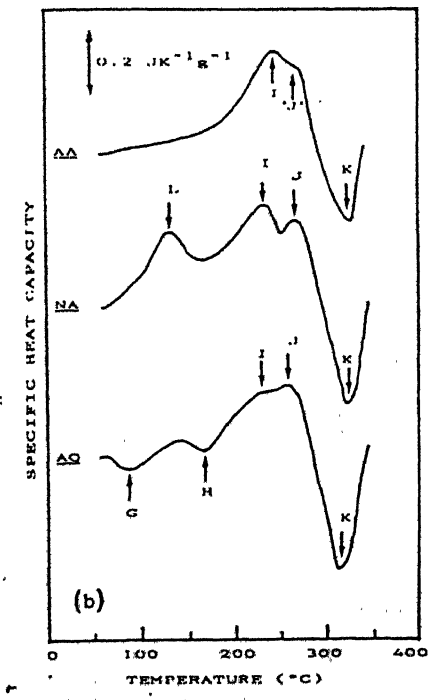

Hence the concentration of Li in solution is greater and closer to that of the δ' solvus: the driving force for dissolution of δ' is least. In the artificially aged condition the volume fraction of δ' should decrease by a factor of 2 between 200°C and 250°C to maintain the equilibrium concentration of lithium in solution so there is the greatest driving force for dissolution in this condition. The TEM observations suggest a decrease in δ' volume fraction although remaining particles retain their size or even coarsen.

Zirconium additon to Al-Li system shows (Fig. 4) absence of 130°C G.P. zone dissolution endotherm. The absence of peak (B) is related to the more δ' formed during quenching: either due to slow quench rate or by additional precipitation of δ' on $\beta'(Al_3Zr)$ particles. However, no definitive TEM observation have been made to support this suggestion. The exotherm (C) is consistent with the growth of a larger size δ'. The remaining endothermic and exothermic behaviour is similar to that reported and discussed for binary Al-Li alloy.

In Al-Cu-Mg (Fig. 5), the endotherm (E) at 220°C is attributed to Al-Cu-Mg G.P. zones dissolution implies that their formation have taken place during quenching. The slight exothermic instability below 100°C is related to formation of there G.P. zones. The exotherm at 270°C (F) indicates precipitation of S phase. In naturally aged condition peak (E) is more pronounced as a result of the increased G.P. zone formation. Whereas artificial ageing completely supresses (E) peak Al-Cu-Mg G.P. zone dissolution peak, indicates complete precipitation of S phase during ageing treatment.

The presence of exotherm (G) at 90°C in Al-Li quaternary (8090) alloy (Fig.6) is related to the same trend observed in Al-Cu-Mg alloy (Fig. 5, (A.Q.sample) Al-Cu-Mg; G.P. zone formation). The presence of Li inhibits their formation during quenching, which occur in Al-Cu-Mg alloys. The explanation is lower free vacancy concentration available because of higher Li-vacancy binding energy. Natural ageing and artificial ageing eliminates (G) peak, presumably G.P. zone formation is complete. Exotherm (H) is formation of δ' precipitates. It is followed by endotherm (I) at 230°C which correspond to the lower temperature range δ' dissolution and Al-Cu-Mg G.P. zone dissolution. The thermal fluctuations at J can be interpreted as the result of superposition of the δ' dissolution and S precipitation reactions. Over the range of the exothermic peak (K), the S precipitation exotherm (270°C) also overlaps at higher temperature with the δ formation exotherm observed at abou

the endotherm at 130°C (L) is present (Al-Li G.P. zone dissolution peak). Presence of Zr in binary Al-Li removes this peak. In that instance, it is suggested that presence of Mg, which reduces Li solubility in aluminium reduces the driving force for G.P. zone formation. However, the presence of 130°C endotherm remains matter of speculation. Artificial ageing at 185°C for 8 hours can not complete S phase precipitation. Further precipitation takes place during DSC heating. It causes the thermal fluctuations at (J) peak, rather than the broadening of D_2 plateau as in Al-Li-Zr. This is in contrast with Al-Cu-Mg system, which suggests that presence of zirconium delays the formation of S phase.

2.3 : Heat Treatment Results

The solutionising temperature of the alloy should be optimum to achieve better balance between dissolution of equilibrium phases and to avoid liquation problem in more concentrated alloy. Surface depletion of solute elements (e.g. Li and Mg) during high temperature treatment should be given proper attention during subsequent processing. In general, higher the solutionising temperature, higher the peak hardness during subsequent artificial ageing. Fig. 7 [61] reflects the effect of solutionising temperature during 190°C artificial ageing of the Al-Li-Cu-Mg-Zr alloy. Solution treatment at 530°C gives maximum peak hardness (142 VPN) during artificial ageing at 190°C.

The effect of three different solutionising temperatures and natural ageing (24 hours) on 8090 alloy (Alloy A) during ageing at 190°C is shown in Fig. 8 [62]. In Figs. 7 and 8, higher solutionising temperature gives higher peak-hardness probably because of two reasons i) degree of dissolution of intermetallics increases and ii) higher density of quenched in vacancies; both the effects aid precipitation of S phase. In Fig. 8, natural ageing shows that it inhibits the onset of overageing.

The effect of stretching on the ageing respose of 8090 at 190°C, is shown in Fig. 9 [63]. The unstretched material reached the peak hardness of 147 VHN after 12 hours. While material with 3% and 6% showed the peak hardness of 153 VHN and 157 VHN, respectively within 8 hours. All hardening curves had a plateau and a measurable decrease in hardness occured after 36 hours. This study shows that increasing the degree of stretch increases the peak-hardness during ageing. This is due to more density of dislocations produced during higher degree of cold work, thereby leading enhanced precipitation of S phase during artificial ageing.

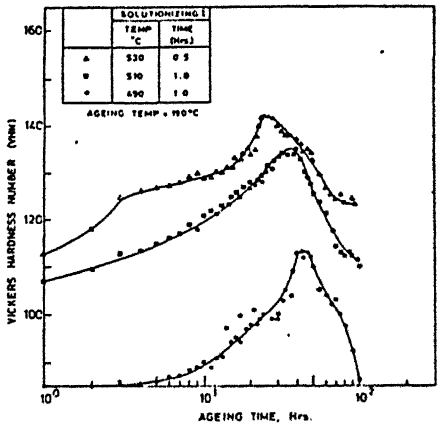

Fig. 7 Age hardening behaviour of Al-Li-Cu-Mg-Zr alloy under different solutionising conditions at 190°C.

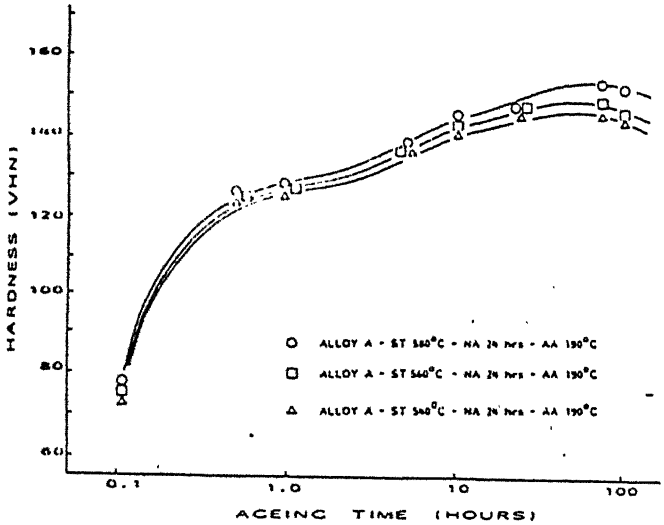

Fig. 8 Ageing curves at 190°C after various solution treatments and natural ageing at 190°C.

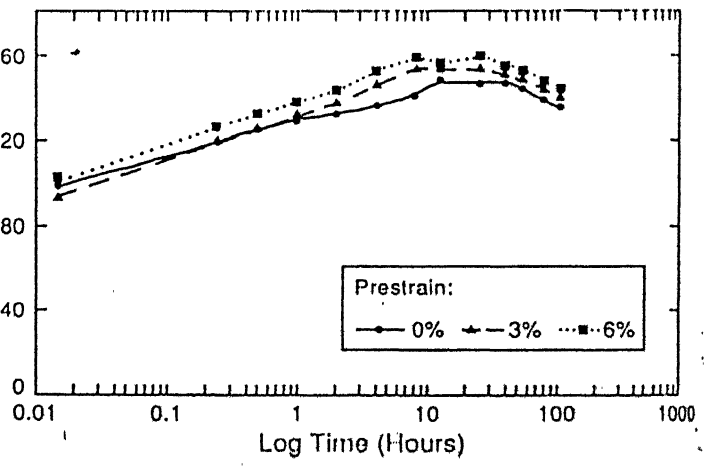

Fig. 9 Age hardening response of 8090 under various stretch conditions.

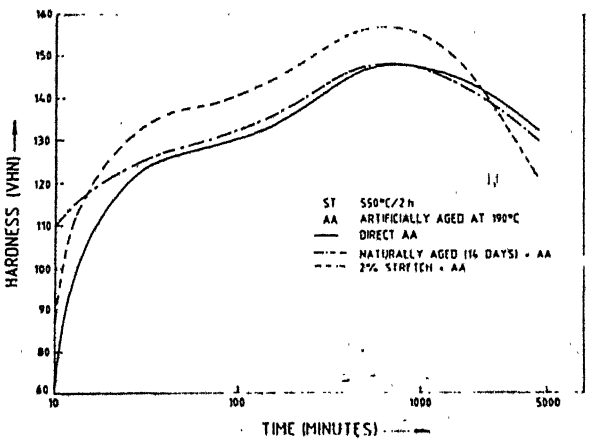

Fig. 10 Ageing response of 8090 under various preageing

Fig. 10 [64] reflects the thermal ageing response of Al-Li-Cu-Mg-Zr alloy at 190°C with different pre-ageing histories (direct ageing, stretching, and natural ageing). Natural ageing period of 14 days seems to decrease the peak ageing time, when compared to 24 hours in (Fig. 8). Higher peak-hardness of a stretched sample during subsequent ageing indicates the similar result as presented in Fig. 9.

2.4 : Processing-Microstructure-Properties

2.4.1 : Al_3Li (δ')

In multicomponent Al-Li alloys, during quenching from solutionising temperature the δ' particles form homogeneously throughout the matrix very rapidly. The ageing treatment to produce significant precipitation hardening involve temperature range of 120°C to 200°C. Artificial ageing time should be less than 24 hrs at 190°C and maximum ageing temperature should be about 190°C to prevent the formation of equilibrium precipitates.

Presence of δ' produces pronounced co-planar slip, and this leads to poor ductility. Co-planar slip also contributes to anisotropy of mechanical properties [6]. Basically, the slip tends to get confined because of precipitate (δ') shearing, which makes further dislocation motion confine to the slip plane and thereby develop a stress concentration, usually at the grain boundaries, which in turn open up grain boundary cracks and induce failure. PFZ adjacent to high angle grain boundary assists this intergranular failure by promoting plastic crack opening in the soft PFZ [65].

The coarsening of δ' during ageing is diffusion controlled process and follows the classical $t^{1/3}$ law, the coarse particles growing at the expense of finer ones. The Lifshitz-Wagner [66,67] theory of particle coarsening yields :

$$r_t^3 - r_0^3 = K\,(t - t_0) \qquad \text{eq.[3]}$$

where K is defined by the expression,

$$K = \left(\frac{8\,e\,C_{eq}\,D\,(V_m)^2}{9\,R\,T} \right) \qquad \text{eq.[4]}$$

where r_0 and r_t are the mean particle radii at the start of coarsening (t_0) and after ageing for time t, respectively. e is the interficial energy of the precipitate, D is the diffusivity of the solute, Ceq is the equilibrium concentration

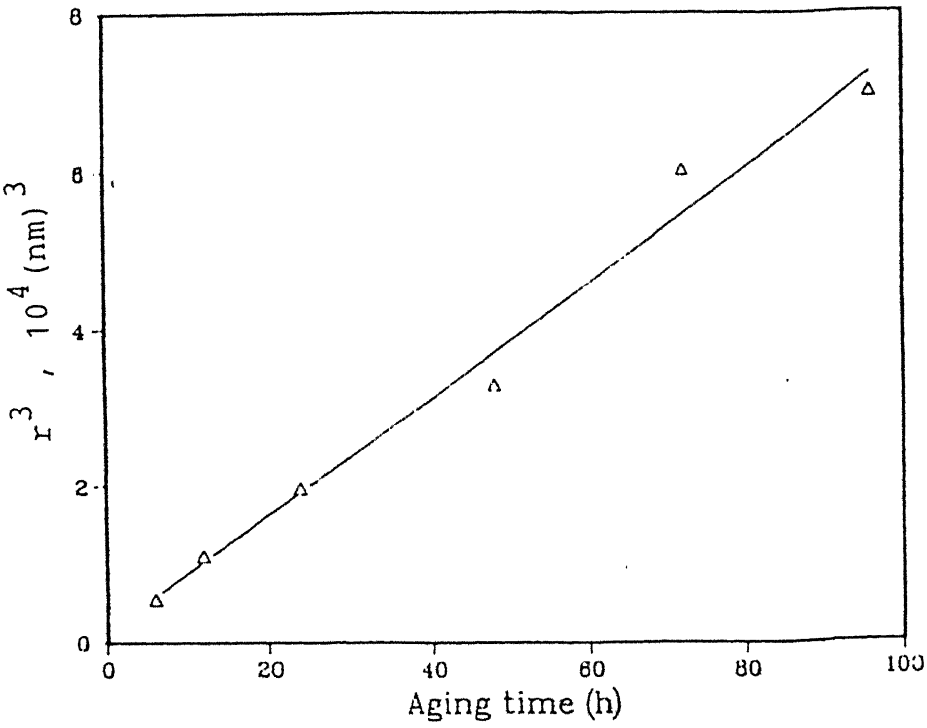

Fig. 11 Coarsening data of δ' particles. (Average particle radius)^3 plotted against ageing time (h).

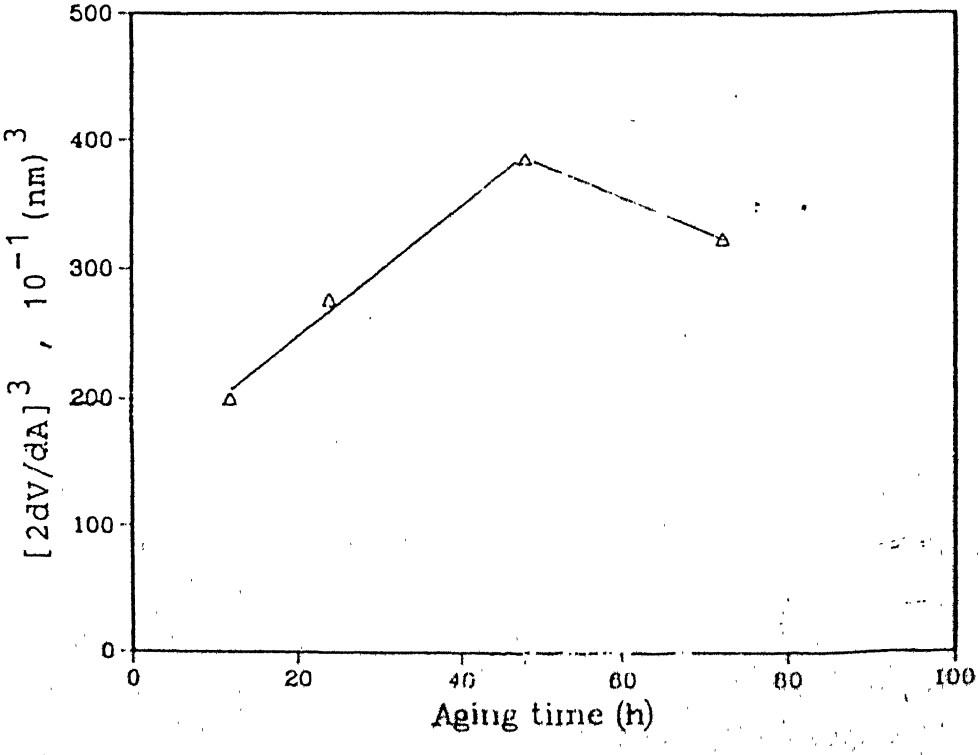

Fig. 12 Coarsening data of S laths. Plot of $[2\,dV/dA]^3$ vs ageing time.

precipitate. The linear relationship between cube of the average particle size and ageing time has been observed in Al-Li-Cu-Mg system by [68] and presented in Fig. 11. The linear curve passes almost through the origin indicating that the nucleation of δ' occurred during the quenching. A similar observation has been made by Noble et al [69] in a series of alloys containing 0, 2, 4, 5, 7, 10 and 14 at% Li. At temperatures greater than 200°C, coarsening deviates from the $t^{1/3}$ law and δ' coarsens more rapidly. The size of δ' is also related to the strength in these alloys. Hardness increases almost linearly with diameter of δ' particles till 14 nm. The coarser δ' particles result in a decrease in hardness value [70].

2.4.2 : Al_3Zr (β')

Addition of Zr (approximately 0.12%) in Al-Li-Cu-Mg gives rise to β' (Al_3Zr) particles, which refine grain size and inhibit recrystallisation taking place during mechanical working and heat treatment [22]. Al_3Zr particles have a pinning effect on grain and subgrain boundries during annealing. The high antiphase boundary energy of the metastable Al_3Zr rules out particle cutting during deformation. The coherent Al_3Zr interface imparts a high drag force to the recrystallisation front since the precipitate matrix interface must change from coherent to semi-coherent or incoherent as the recrystallisation front passes. In other case the particles must dissolve and re-precipitate after the boundary passes, if the orientation relationship is to be maintained; either of these two process requires considerable energy. However, inhibition of recrystallisation gives rise to highly textured structure which promotes anisotropy in the material.

The Al_3Zr phase is proved thermodynamically stable in PFZ. Thus PFZ is strengthened, and the alloy is less prone to intergranular failure [28]. It also improves the toughness and stress corrosion resistance [71]. Sastry et al. [72] found the yield stress of Al-3%Li-0.3%Zr alloy at 250°C to be 180-200 MPa higher than that of the Al-3%Li because of the presence of 1-2 μm subgrains in the Zr containing alloy.

2.4.3 : Al_2CuMg (S)

In quaternary alloys containing Cu and Mg, modification of slip behaviour can be induced by the precipitation of S phase. In the solution-treated condition, the subgrain interiors are generally free from the dislocation loops and helices in Al-Li alloys. The absence of these defects is attributable to the high lithium vacancy binding energy (0.25-0.26 eV) [42,73]. In dilute alloys ageing in the range of 170°C-190°C gives rise to precipitation of T_1 and S phases at dislocations and sub

grain boundaries within 24 hrs. thereby indicating that S precipitation is sluggish

S phase is effective in breaking up the coplanar slip and consequent strain localization. It changes failure mechanism from one of the long range planar shear to one involving substantial amounts of ductile tearing. In addition to substaintial improvement in toughness, the role of S phase in promoting homogeneous deformation has a second consequence; the material is capable of displaying isotropic properties even though a strong texture is present in the Zr refined material (unrecrystallized). Texure development alongwith planar slip is harmful to toughness.

Homogeneous precipitation of S phase during commercially viable age hardening treatments is not possible due to low density of quenched in defects to act as nucleation sites [48]. The use of pre-ageing stretch, natural ageing prior to artificial ageing, and slow heating to final ageing temperature results in relatively hetrogeneous precipitation of fine laths of S phase.

2.4.3.1 : Effect Of Cold Working

S phase nucleates preferentially on stray dislocations and upon subgrain boundaries, and a more uniform distribution is produced if the solution treated material is plastically stretched prior to ageing. The primary role of dislocations introduced during deformation is to provide nucleation sites for S phase [62,74]. The application of increasing stretch appers to produce an increasing size of S and T_1 (Al_2CuLi) phase particles in 8090. However, The increased precipitation of S at the expense of T_1 results in a more homogeneous distribution of slip, and give rise to improved toughness and more isotropic properties in a texured sheet product [6]. T_1 is relatively ineffective in breaking up co-planar slip.

Prefered precipitation of S phase can be favoured by choosing appropriate Cu:Mg content. It may be inferred that the dislocations introduced also act as pipe diffusion channels for Mg and Cu, so that enhanced particle growth rates determine the particle size [73]. In considering the stretched samples, an increase in yield stress is apparant, but it is notable that the 7% stretch results in a structure of lower yield stress than 4% stretch. This presumably is because of softening arising from the increase in size of the S phase particles (and thus coarser dispertion) outweighs the contribution to the strength from the dislocation structure. The effect of pre-ageing stretch on ageing curve is shown

in Figs. 9 and 10 in section 2.3. However, this pre-ageing stretch method is inappropriate in commercial practice, where final alloy product may require to be re-solution treated before ageing.

2.4.3.2 : Effect Of Natural Ageing

The solution treated and quenched material is retained at room temperature for natural ageing. Microstructurally the observable changes are the development of δ' dispersion and the formation of dislocation loops and helices throughout the matrix. In addition to providing hetrogeneous nucleation sites for S phase via dislocation loops and helices produced, natural ageing promotes the formation of S phase upon subsequent artificial ageing. Quenched in vacancies are bound to lithium atom clusters (δ') in the as quenched condition. During natural ageing, the vacancies are released and they may be responsible for homogeneous precipitation of S phase during artificial ageing. The existance of percursor to S phase is not reported during natural ageing by TEM. But the DSC thermogram of 8090 samples, 90 days naturaly aged showed the absence of formation peak for Al-Cu-Mg GP zone, which occurs in as quenched sample [40].

The study by [62] has shown that in 8090 samples subjected to natural ageing for 24 hours, the initial artificial ageing response was unaltered compared to directly artificially aged sample. But the natural ageing has inhibited the onset of overageing. Wheras in case of 1400-1800 hours natural ageing for the same sample showed overageing is inhibited and the overall hardness values are higher. Overageing is inhibited probably due to more widespread precipitation of S phase as compared to artificially aged sample without natural ageing. In 1850 hours naturally aged samples S phase was observed within 4 hours at 190^{o}C. In general, increasing the natural ageing period results in an increase in the size of S particles developed for any artificial ageing treatment [62]. The study by Ozbilen et al. [75] has shown the presence of thin needles of S phase after prolonged natural ageing (15 months at room temperature) in Al-0.82% Li-1.96% Cu-0.84% Mg alloy. However, it is clear that to promote widespread S phase, longer natural ageing period is required. There arises the question of industrial acceptance.

2.4.3.3 : Effect Of Slow Heating Rate

It has been shown that slow heating to the ageing temperature can lead to a better balance of tensile strength and toughness in 8091 (Al-2.40% Li-2.07% Cu-0.76% Mg-0.11% Zr) alloy [76]. The mechanism of enhanced precipitation of S phase by slow heating is probably related to the release of vacancies. It has been

suggested that the vacancies trapped in solid solution on quenching (bound to δ') are released as the δ' grows [48]. In the slow heating, as the temperature increases, δ' grows and vacancies are released. The vacancies around Al_3Zr particles (due to enhanced precipitation of δ' around Al_3Zr), condense to form loops which can expand by capturing more vacancies on ageing and provide sites for subsequent nucleation of S laths. The slow heating to the ageing temperature perhaps results in a more controlled release of vacancies as the δ' precipitates coarsen, (compared to that for direct ageing), and as ageing progresses, homogeneous S is also formed more readily as extra vacancies which have not condensed to form loops become available; i.e. at a temperature high enough for precipitation of S phase, the vacancies assist the formation of S phase rather than to form loops, perhaps by aiding the widespread formation of a precursor to the S phase.

The increase in strength obtained by slow heating to 190^{0}C in 8091 alloy must be due to the additional time at elevated temperature before final artificial ageing temperature is reached [75]. The δ' size is larger for a given time at the actual temperature (slow heating to 190^{0}C and holding for 10 hours results in δ' with size of 25 nm, as compared to direct ageing at 190^{0}C for 16 hours resulted in δ' size of 20 nm). This means that for a required δ' size (strength level), a shorter time at the ageing temperature is needed. It was hoped that this would reduce the amount of grain boundary precipitation, but the evidence for this was inconclusive. The lower value of proof stress obtained in the same investigation suggests that ramping to the ageing temperature may not benefit as effective as cold working, but it improves ductility and toughness. The enhanced precipitation of S phase may improve resistance to SCC. It has been shown that cold working prior to ageing decreases SCC suseptibility, and it is believed that this is due to the precipitation of S phase on the dislocations within grains, reduces the driving force for preferential anodic dissolution at grain boundaries where there are copper-rich particles [77]. This method seems to be best alternative, where natural ageing time or cold working of the component before artificial ageing is not feasible.

The study by Ahmed et al. [68] on the 8090 alloy has shown that S phase forms by hetrogeneous nucleation on dislocation loops and helices. The average particle volume V and surface area A, were calculated from the S laths. The effective particle radius re is, according to Wagner [67],

$$r_e = \frac{2\,(dV)}{(dA)} \qquad \text{eq.[5]}$$

A plot of r_e^3 vs ageing time (Fig. 12 on page 22) [68] is a straight line for ageing times up to 48 hours. For ageing time more than 48 hours the coarsening rate is reduced. The value of K is given by the same equation (eq. 4) applied for δ' coarsening (see page 21).

2.4.4 : Grain Boundary Precipitates

The presence of grain boundary precipitates is one major source for the intercrystalline failure. Premature failure could occur via void formation at the hard grain boundary precipitates, facilitated by the surrounding soft PFZ material [78,79]. In any event, more and larger G.B. precipitates, as seen with increasing ageing time, produce worse ductility value. This is supported by the observation that the ductility is decreasing with ageing time: it is clear that the PFZ width increases with ageing time, and that a wide PFZ should give higher ductility than the narrow one [77,80,81] so that the decrease in ductility with ageing time can not be attributed to widening of the PFZ.

The grain boundary precipitates can be broadly classified into two groups: firstly, the coarse particles, which form during solidification and survive the subsequent heat treatments and secondly, the particles which precipitate during artificial ageing. Former type of precipitates include iron and silicon phases and T_2 phase. The iron and silicon phases are discussed in section 2.4.6. Formation of latter type of precipitates depends on ageing temperature and time, alloy composition, and to some extent preageing parameters. The age hardening phases like T_1 and S which form at low angle grain boundaries will not be discussed.

Equilibrium δ has been reported as the principle high angle grain boundary phase in all Al-Li alloys [82]. Due to its reactive nature, retention of δ during the preparation of thin foils for TEM observation is difficult. Hence, its presence at grain boundaries is reported only by a few investigators [18]. The presence of this δ leads to δ' PFZ at the grain boundary, which causes localised lithium denudation.

In magnesium containing Al-Li alloys, Harris et al. [18] identified coarse Al_2LiMg precipitate at grain boundaries, which is favoured by increasing magnesium content. The other grain boundary precipitate reported in 8090 and 8091

alloys is icosohedral I-phase ($Al_5Cu(Li,Mg)_3$) [83]. This phase forms during the quench and grows as snake-like precipitates along grain boundaries. Recently, the detailed investigation of Owen et al.[84] on grain boundary precipitates in AA 8090 shows no evidence of stable δ in the peak and over aged conditions. The author has concluded that an I phase reported by Cassada et al. [82] is the major grain boundary precipitate and responsible for δ' PFZ formation. Other complex C phase has been reported in overaged alloys [85]. All the above mentioned G.B. precipitates are detrimental to the fracture toughness. The study by Ahrens et al. [86] reports that 6% stretch prior to ageing does not alter the distribution of grain boundary precipitates.

The deterimental effect of (Na, Ca, K, and S) tramp elements is well established. The alkali metals form aggregates of liquid at room temperature and assist fracture at grain boundary. However, it is found that the fracture toughness of the material increases, when tested at cryogenic temperatures.

T_2 : (Al_6CuLi_3) Phase

It preferentially precipitates at grain boundaries, which is deleterious to fracture toughness. Its precipitation increases the δ' PFZ width. The strenthening effect of T_2 is very low. It behaves as the Al_2LiMg phase, which causes no hardening increment in overaged alloys.

2.4.5 : Precipitate Free Zones (PFZs)

The observation of Precipitate Free Zone (PFZ) adjacent to grain boundaries is a common occurrence in many age hardenable aluminium alloys. Poor ductility and fracture properties of Al-Li alloys have been linked to the presence of PFZ's in the microstructure [87]. When Al-Li alloys with sufficient solute are quenched from the single phase field and artificially aged, the δ' precipitates homogeneously in the matrix. During artificial ageing the δ' particles begin to coarsen and the time dependent coarsening rate follows Ostwald ripening kinetics [88]. In addition to the coarsening of δ' particles in the matrix, preferential growth of the equilibrium phase δ (AlLi) occurs on the grain boundary. The solute necessary for the continued growth of δ is supplied by the dissolution of δ' particles in the vicinity of the grain boundaries [89,90].

PFZ formation has been explained either by a vacancy depletion or a solute depletion mechanism [91,92,93] In case of vacancy depletion, a vacancy concentration profile develops near the grain boundaries in a solution heat

treated and quenched alloy. At a temperature above the critical temperature for homogeneous nucleation, an excess critical vacancy concentration is required for the nucleation of the precipitating phase. Near the grain boundaries, the vacancy concentration is less than the critical value, and hence no precipitates form and a PFZ results. In the solute depletion mechanism, the solute preferentially segregates to the grain boundaries after solution heat treatment and quenching. The solute concentration profile forms near the grain boundaries. A certain minimum solute concentration is required for the homogeneous nucleation of the precipitating phase. Therefore, the presence of a PFZ in this case can be explained by an argument similar to that for the vacancy depletion machanism.

The PFZ width (h) in the unrecrystallised Al-Li alloys (containing Zr) is quiet non-uniform. Some boundaries are associated with very large PFZ's while no PFZs are observed at others. The average PFZ width in the recrystallised alloy, however increases parabolically with time. The PFZ growth rate is more in unrecrystallised alloys than in the recrystallised Al-Li alloys (containing Mn). It has been found that a relationship of the type $h = K\ t^n$ is valied [94]. Where, h is half PFZ width and t is the ageing time. The parameter n is reported to be between 0.33 to 0.5. The parabolic dependence of PFZ growth on time suggests that this process is controlled by the diffusion of Li to provide the solute necessary for the continued growth of δ particles at the grain boundaries. On the basis of diffusion controlled process [89,95] reported that,

$$h = 2\ b\ (Dt)^{1/2} \qquad \text{eq.[6]}$$

where, b is obtained from the transcendental equation,

$$\frac{C_{\delta'} - C_{\delta}}{C_0 - C_{\delta'}} = \left(\pi\ b\ \exp(b^2)\ \mathrm{erf}(b) \right)^{1/2} \qquad \text{eq.[7]}$$

In the above equation, D is the interdiffusion coefficient, C_{δ} and $C_{\delta'}$ are the concentration of Li in the matrix in equilibrium with the δ and δ' phases respectively, and Co is the original composition of the alloy. But this formulation involves the assumption that the grain boundaries act as an infinite sink for the solute and neglects the mass balance related to the formation of δ

Fig. 13 Schematic diffusion profile representing PFZ growth process in Al-Li alloys

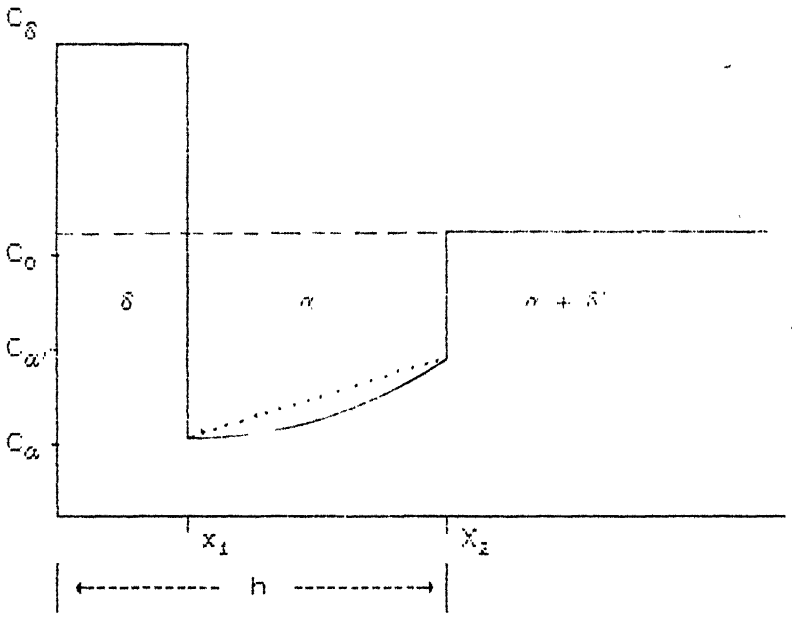

Table IV Insolubles in Al-Li alloys

Phase	Crystal structure	Lattice parameter (nm)
Al_7Cu_2Fe	Tetragonal	$a = 0.6336$, $c = 1.487$
$Al_{23}CuFe_4$	Orthorhombic	$a = 0.7664$, $b = 0.6441$, $c = 0.8778$
$Al_{20}Cu_2Mn_3$	Orthorhombic	$a = 2.411$, $b = 1.251$ $c = 0.72$
Al_5FeSi*	Monoclinic	$a = 0.612$, $b = 0.612$, $c = 4.15$, $\beta = 91°$
Al_8Fe_2Si*	Hexagonal	$a = 1.23$, $c = 2.63$
$Al_6(Cu, Fe, Mn)$	Orthorhombic	$a = 0.646$, $b = 0.746$ $c = 0.879$
$Al_{12}(Fe, Mn)_3Si$*	Cubic; space group $Pm\,3$	$a = 1.265$

*10 different Al-Fe-Si phases have been reported in the literature (P Skjerpe 1987 *Metall. Trans.* A18 189); one or more of these phases may appear in the commercial Al-Li alloys

particles at the grain boundary. The study by Jha et al. [93] (Fig. 13) considers the mass balance and the solution for the PFZ width by The Linear Solution Method is as follows,

$$h = \left(\frac{(C_{\alpha'} - C_{\alpha})\ (2C_o - C_{\alpha'} - C_{\alpha})}{(C_{\delta} - C_{\alpha})\ (C_{\delta} - C_o)} \right)^{1/2} (D\ t)^{1/2} \qquad \text{eq.[8]}$$

The activation energy determined for the PFZ growth process is 144 kJ/mol, which agrees with the activation energy for the diffusion of Li in to α - Al (136 kJ/mol) [96].

The occurrence of S PFZ has been reported in 8091 Al-Li quaternary alloy ~ 0.5 μm [76]. Another S PFZ has been reported in 8090 Al-Li alloy by Shakesheff et al. [97], to be (about 0.1 μm) adjacent grain boundaries. But, absence of S PFZ adjacent to high angle grain bourndary is reported by Sinko et al. [63] in stretched 8090 alloy. The explanation is the dislocations in the vicinity of grain boundary serve as competing nucleating sites for the S precipitates and decrease the probability of developing wide PFZ's due to perferential grain boundary precipitation.

2.4.6 : Nature Of Insolubles

Impurities such as iron and silicon present in commercial Al alloys can give rise to various insoluble particles (inclusions) which are shown in Table IV [58]. The AlLiSi phase occurs in Si containing alloys. The insolubles are usually coarse and have comolex crystal structure. They offer heterogeneous sites for formation of δ (AlLi) and hence allow the formation of a precpitate-free zone (PFZ) in the matrix. They have a significant influence on precipitation and recrystallization characteristics in addition to the adverse effect on ductility and fracture toughness. Rapid solidification technique can lead to refinement in size of these insolubles. The presence of copper and lithium in insolubles would reduce the amount of these elements available for the formation of T_1, S and δ' thereby causing a decrease in their volume fraction and therefore to precipitation hardening. Hence, stringent quality control of the base metal Al has to be exercised, keeping low levels of these elements (« 0.2% Si and ‹ 0.3% Fe).

2.5 : Scope Of The Present Work

In the present alloy system (8090) Cu and Mg concentrations are enough to provide the critical solute supersaturation in the matrix. The natural ageing and slow heating prior to artificial ageing are expected to influence concentration of free vaccancies and can affect the S phase distributuion.

Ageing respose at room temperature and at low temperatures ($50^{o}C$ and $75^{o}C$) is studied to understand low temperature developments in the microstructure. Artificial ageing treatments are chosen in the temperature range of $160^{o}C$ to $190^{o}C$. The comparison of δ' precipitate size, S phase distribution and δ' PFZ width by TEM micrographs are expected to provide valuable imformation. DSC analyses is used to investigate Al-Li G. P. zone formation period during the natural ageing. Various age hardening practices are evaluated via Vickers hardness measurment.

CHAPTER III
EXPERIMENTAL PROCEDURE

3.1 : Material Studied

The 8090 alloy used in this investigation was purchased by D.M.R.L., Hyderabad from British Alcan Limited (U.K.). The alloy received was in the form of 45 mm thick plates and in T 851 condition. (T 851 cold worked prior to artificial ageing). The chemical composition in weight percent is as follows :

(Al- 2.42%, Li- 1.00%, Cu- 0.73%, Mg- 0.12%, Zr)

with H ~ 3 ppm., 0.02% Fe, Si < 0.01%, Na < 10 ppm, Ca < 10 ppm, and K < 20 ppm.

3.2 : Heat Treatment

Samples of roughly 20 mm cube were cut on a mechanical power saw. The heat treatment schedule was as follows. The abbreviations A.A., N.A., and S.H. mean artifitial ageing, natural ageing and slow heating, respectively.

a) Solutionised at 550^{0}C for 2 Hrs., and water quenched.

b) A.A. according to Table 5.

c) N.A. (12 Days) + A.A. according to Table 5.

d) N.A. (42 Days) + A.A. according to Table 5.

e) Heated to ageing temperature with controlled heating rate (10^{0}C/Hr.) + A.A. according to Table 5.

Table 5 : Ageing temperatures and time

Ageing Temperature In ^{0}C	Ageing Time In Hrs
160	196
170	89
180	42
190	20

Solution treatment was carried out in a vertical steel tube furnace. The temperature was controlled by APLAB Temperature Controller with an accuracy of +/- 3^{0}C. Solutionising Temperature and time were chosen based on literature [62]. A surface layer of about 0.3 mm was removed from the solutionised samples because of Li and Mg depletion from this zone. After solution heat treatment the samples were either placed in the oven for artificial ageing or for natural

ageing at room temperature (about 30^{0}C). The natural ageing study of the as quenched material was done by hardness (VPN) measurements up to 100 days.

Hardness-ageing time data were determined for samples with different pre-ageing history : as-quenched, naturally aged for 12 days and slowly heated from room temperature to 190^{0}C.

The ageing time for 190^{0}C was chosen to be 20 hours to give peak hardness based on our work and the associated data in literature [62]. Peak ageing times for other temperatures were estimated based on equivalent solute (Li) diffusion distances $(D\ t)^{0.5}$.

The heating rate control in (e) [refer section 3.2] heat treatments was achieved by a programmable temperature controller. The temperature was controlled with the accuracy of +/- 1^{0}C. The print-out of actual and desired temperatures was taken at the interval of 10 minutes.

3.3 : Low Temperature Ageing

The alloy was solutionised at 550^{0}C for 2 hrs. and water quenched. The ageing curves at 50^{0}C and 75^{0}C were determined and the high temperature ageing (190^{0}C, 20 hrs.) was done on selected (peak-aged) samples. The main purpose of this study was to find short time equivalent treatments for natural ageing of the alloy.

3.4 : Hardness Measurement

Vickers Pyramid Hardness with a 10 Kg load was measured on samples heat treated under various conditions, as shown in Table 6. The samples were lightly polished on 1/0 paper polshing paper to remove the oxide surface layers produced during heat treatment. Typically five indentations were made for each test.

3.5 : Differential Scanning Calorimetry (DSC) Analyses

The DSC provides imformation complementary to that obtained by means of common metallurgical techniques. In addition precipitation of phases too fine to be observed on a conventional TEM can be detected on a DSC plot with the help of peaks present.

The present research has used DSC to investigate the effect of natural ageing and slow heating on phase transformations. The DSC analyses were done on samples according to Table 6. The samples were cut in *Buehler Isomet*^{TM}, *Low Speed Saw* and weighed to an accuracy of +/- 0.01 mg. on digital weight balance. DSC analysis was undertaken in a *'Du Pont Instuments - 910 Differential Scanning*

Calorimeter' under following conditions :

a] Weight of the sample 25 - 30 mg.

b] Heating rate 10^{0}C/min.

c] Temperature range 30^{0}C - 500^{0}C.

3.6 : Optical Microscopy

Optical microscopy was done to select planes perpendicular to the rolling plane for further TEM work. As the number of grains in L-T direction were more, it was easier to study Precipitate Free Zone (PFZ) adjacent to high angle grain boundary. A 'CARL ZEISS' optical microscope was used and the specimens were etched with *Keller's reagent* (190 ml H_2O, 10 ml HNO_3, 6 ml HCl, and 4 ml HF.)

3.7 : Transmission Electron Microscopy

Transmission Electron Microscopy (TEM) was done on samples heat treated according to Table 6. The TEM sample preparation was of two stages and features observed were the following :

3.7.1 : Sample Preparation

After the observation in the optical microscope the L-T direction was defined. A thin slice of ~ 200 μm. was cut in Buehler Isomet^{TM}, Low Speed Saw. This thin slice was mechanically polished on 1/0 polishing paper to reduce the thickness to about 50 to 80 μm. 3 mm discs were punched out from the slice.

These discs were electropolished in *E.A. Fischione* twin jet polishing Instrument. The flow rate of the electrolyte, temperature and voltage were the variables. The electrolyte was 30% nitric acid and 70% methanol maintained at -30^{0}C. The operating voltage was 12 V. The formation of hole in the disc was detected with the help of a light beam and photo cell.

3.7.2 : Features Examined

Transmisson Electron Microscopy was carried out on a 'PHILLIPS EM 430 T' TEM operating at 300 kV. The δ' dark field image was formed with the use of (100) superlattice reflections. Whereas δ' PFZ micrographs were taken in the bright field in the same direction as δ' observed. Care was taken to align the grain boundaries parallel to the electron beam direction, so that a true width of the PFZ was photographed. The δ' PFZ width measurement was done on atleast four different grain boundaries for each ageing condition. S phase distribution within the grain was also observed under bright field image. To facilitate comparison between the microstructuers examined, all the δ', δ' PFZ, and S micrographs

presented were taken under the same condition as mentioned above.

Table 6 : Experimental work performed

R.T. : room temperature Y : carried out

Condition	TEM	DSC	Hardness
1) As received	Y	Y	Y
2) As Quenched	Y	Y	Y
3) 19 N.A.		Y	Y
4) 42 N.A.		Y	Y
5) 57 N.A.	Y	Y	Y
6) 190 A.A.	Y		Y
7) 12 N.A. + 190 A.A.	Y		Y
8) 42 N.A. + 190 A.A.	Y		Y
9) 30 to 190 slowly heated		Y	Y
10) S.H. from R.T. + 190 A.A.	Y		Y
11) 180 A.A.			Y
12) 12 N.A. + 180 A.A.			Y
13) 42 N.A. + 180 A.A.			Y
14) 30 to 180 slowly heated			Y
15) S.H. from R.T. + 180 A.A.			Y
16) 170 A.A.			Y
17) 12 N.A. + 170 A.A.			Y
18) 42 N.A. + 170 A.A.			Y
19) 30 to 170 slowly heated			Y
20) S.H. from R.T. + 170 A.A.			Y
21) 160 A.A.	Y		Y
22) 12 N.A. + 160 A.A.	Y		Y
23) 42 N.A. + 160 A.A.	Y		Y
24) 30 to 160 slowly heated			Y
25) S.H. from R.T. + 160 A.A.	Y		Y

CHAPTER IV
RESULTS AND DISCUSSION

The work presented in this chapter is concerned with the effect of different pre-ageing parameters on age hardening characteristics of the 8090 Al-Li alloy. The results presented are in terms of ageing curves, DSC thermograms, and transmission electron micrographs. Results on characterisation of the 8090 alloy in the as-received (T851 temper) and the re-solution treated condition are presented initially. This is followed by a discussion of the effect of various heat treatments on the hardness and DSC response. Finally specific microstructural features such as δ', S and T_1 precipitates are presented and their relationship with the heat treatment variables are discussed.

4.1 : Characterisation Of The As Received (T851) Sample

The as received material (8090 alloy) was in T 851 (solutionised, cold worked and artificially aged) condition; the hardness was 165 VPN.

In all the DSC plots presented here, upward peaks indicate exothermic reaction and downward peaks indicate endothermic reaction. DSC thermograms give indirect evidence regarding precipitate formation and dissolution, and direct TEM observations are necessary for confirmation of the various effects.

The DSC thermogram of as received material is shown in Fig. 14. A shallow endotherm (L) occurs at 120^{0}C . This could be due to Al-Li G. P. zones dissolution [41] or retrogression of fine δ' [45]. During artificial ageing the Al-Li G.P. zones are replaced by δ'. Hence the presence of (L) peak suggests that this process is not completed during artificial ageing. One possibility is the formation of δ' at room temperature after the artificial ageing, as suggested by [46]. Which could dissolve on heating during DSC. The (L) peak is followed by an exotherm at 170^{0}C (H), which is generally attributed to the precipitation of δ' [39,41,45]; this confirms that δ' formation is incomplete in the as received sample. The subsequent prominent endotherm at 230^{0}C (I) has been attributed to δ' dissolution. An exothermic peak (K), present at 330^{0}C, is reported to be due to precipitation of δ phase. Over the range of the exothermic peak (K) S precipitation exotherm overlaps it around 330^{0}C [40].

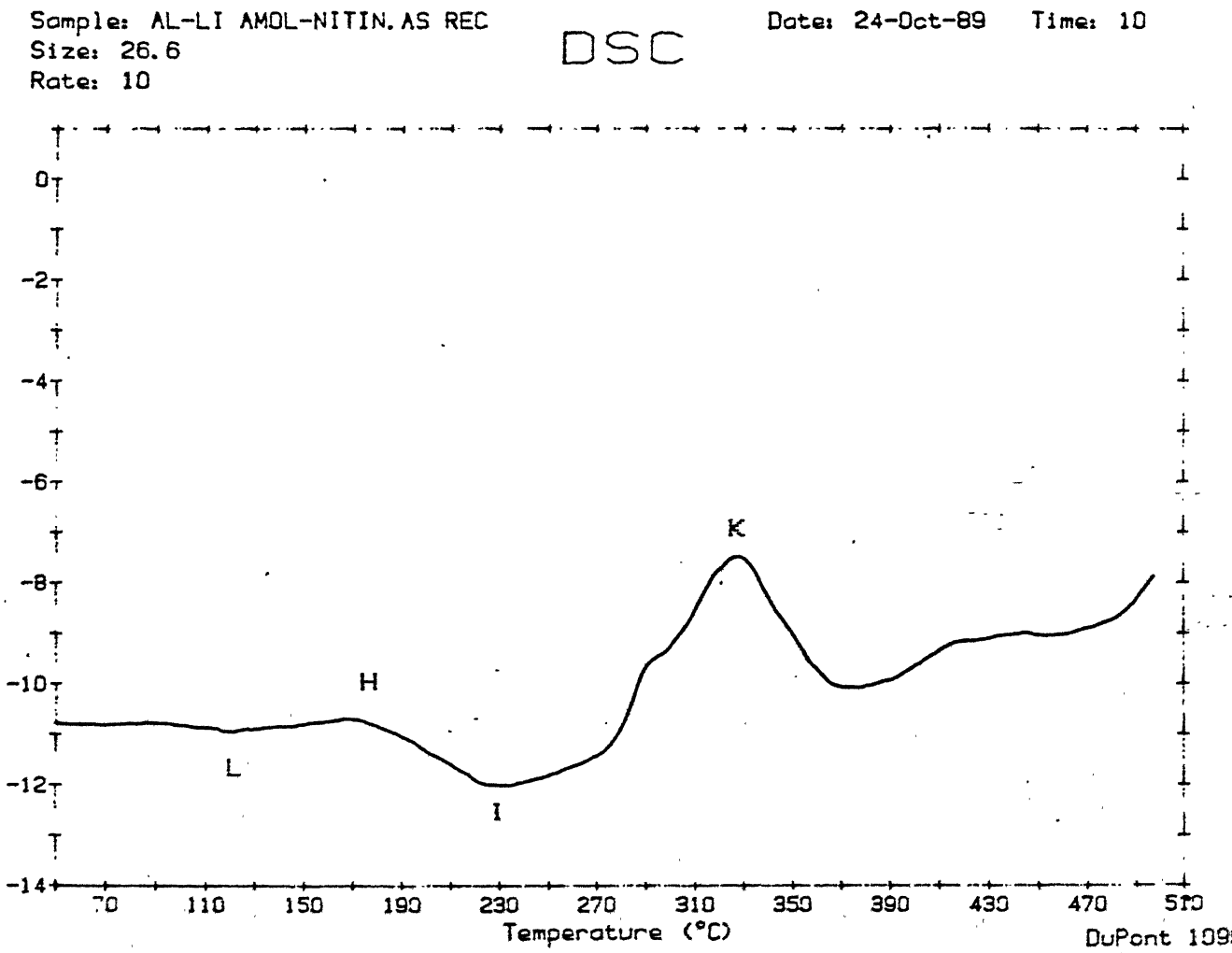

Fig. 14 : DSC thermogram of as received sample

Transmission electron micrographs of the as-received sample are shown in Figs. 15, 16 and 17. A uniform distribution of fine δ' precipitate (~15 nm dia.) is seen in Fig. 15, while a PFZ along the grain boundary is clearly seen in Fig. 16. The PFZ width in this condition (about 0.017 μm) is narrower than what is found in the present investigation for various ageing treatments (see table XI). When these results are co-related with DSC data pesented in Fig. 14, it can be concluded that the as received sample was underaged (peak ageing should supress (L) and (H) peaks in DSC). But in this conditon these peaks are present, although of a small magnitude. The higher hardness as compared to peak-aged samples in this work (see table IX) and uniform distribution of S phase in the matrix (Fig. 17) is believed to be due to a network of dislocations generated during cold working prior to artificial ageing.

4.2 : Characterisation Of The Solution Treated Sample

The as received sample was solutionised at 550^{0}C for 2 hours and quenched into cold water. The as quenched hardness of the material was 68 VPN.

The sample was unavoidably delayed for 1 hour at room temperature prior to thermal analysis. The DSC thermogram is shown in Fig. 18. Two prominent exothermic peaks at 90^{0}C (G) and 170^{0}C (H) are seen. The presence of exotherm (G) is related to the formation of G.P. zones of the S phase, and is similar to that observed by Mukhopadhyay et al. (Fig. 6, Chapter II) [40]. Exotherm (H) is due to the formation of δ' precipitates. It is followed by a slightly endothermic behaviour with two plateaus at 230^{0}C (I_1) and 270^{0}C (I_1). /I_1/ peak corresponds to the lower temperature range δ' dissolution and G.P. zone (Al-Cu-Mg) dissolution [40]. The magnitudes of I_1 and I_2 peaks are smaller and further work (preferably TEM) is essential to understand this portion of DSC. Broadening of (I) peak has been discussed in section 2.2.4. in Chapter 2. As pointed out earlier the prominent exotherm around 320^{0}C (K) is believed to be due to S and δ precipitation.

Dislocation loops formed by the condensation of vacancies and superdislocations are the prominent features of the as-quenched sample (Figs. 19-21). Some of the dark features could be β' particles. But, it was not been possible to establish this unambiguously by electron diffraction. Also, it was not possible to observe δ' precipitates in either the dark field or the bright field modes. But the presence of superlattice reflections in the electron diffraction patterns indicates the presence of δ' in the as solutionised condition.

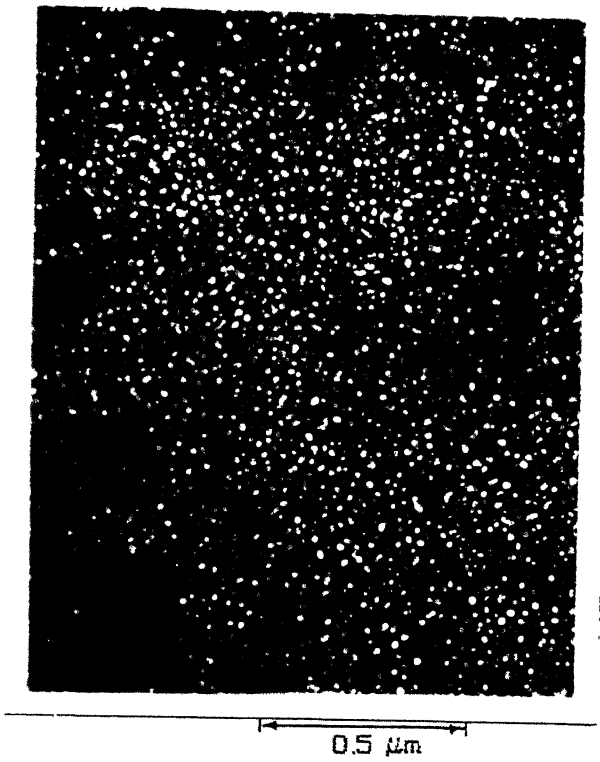

Fig. 15 : D. F. δ' micrograph of as received sample.

Fig. 16 : B. F. δ' PFZ micrograph of as received sample.

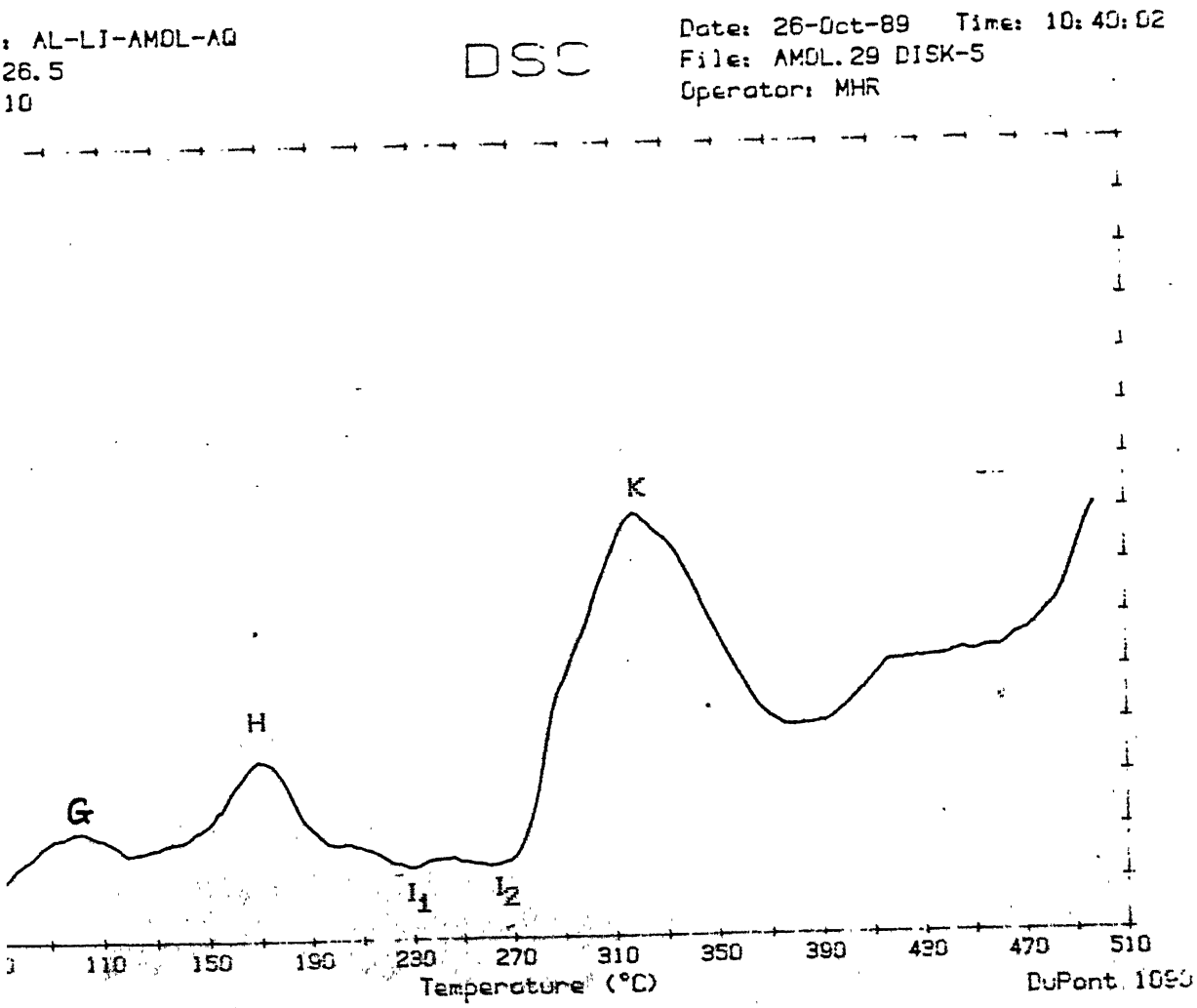
: AL-LI-AMDL-AQ
26.5
10
DSC
Date: 26-Oct-89 Time: 10:40:02
File: AMDL.29 DISK-5
Operator: MHR
G
H
I1
I2
K
110
150
190
230
270
310
350
390
430
470
510
Temperature (°C)
DuPont 1090

Fig. 19 : Dislocation structure in as quenched sample. (Solutionised at 550^{0}C, 2 hrs.)

Fig. 20 : Dislocation structure in as quenched sample. (Solutionised at 550^{0}C, 2 hrs.)

4.3 : Effects Of Preageing Treatments On Hardness And DSC Behaviour

4.3.1 : Natural Ageing

The natural ageing response (room temperature storage) of 8090 alloy is shown in Fig. 22. The as quenched hardness was 68 VPN. There is clear indication of a rapid increment in hardness during the first 12 days. This increase in hardness is due to δ' growth in the matrix. The hardness varies in between 109 - 114 VPN upto 77 days. After 77 days hardness decreases below 109 VPN possibly because of δ' coarsening. This could be the onset of overageing at room temperature.

Figs. 23, 24, and 25 are thermograms of samples naturally aged for 19, 42 and 57 days respectively. Natural ageing eliminates (G) peak in all the samples, indicating that G.P. zone formation (Al-Cu-Mg) is complete. In Fig. 23 prominent (H) peak at 170^{0}C is present, which demonstrates that δ' formation occurs during DSC even after 19 days of natural ageing. Except for the 19 days naturally aged sample, prominent (L) peak at 130^{0}C is present in the other two thermograms [Figs. 24 and 25], which is Al-Li G.P. zone dissolution peak. Increased natural ageing gives larger (L) peak, probably because of more Al-Li G.P. zone formation. Presence of (L) peak after 90 days natural ageing is reported in literature [40]. Our study shows that 42 days natural ageing gives rise to a similar peak. So, samples with 42 days natural ageing were selected for further high temperature artificial ageing.

δ' dissolution peak around 230^{0}C (I) is present in Fig. 23, whereas Figs. 24 and 25 show thermal fluctuations (I_1 and I_2) in the temperature range of 230^{0}C to 270^{0}C before the exothermic reaction at 320^{0}C (K). The thermal fluctuations at I can be interpreted as the result of superposition of the δ' dissolution and S precipitation reactions. In all the three thermograms (K) peak around 320^{0}C is associated with δ formation.

The microstructure of the sample naturally aged for 57 days is shown in Figs. 26 and 27. Helical dislocations and dislocation loops are the important features of these micrographs. A prominent feature of natural ageing is the growth of δ', which releases the vacancies bound to lithium atoms in solution. When a sufficient supersaturation of freed vacancies is obtained some of them precipitate in the matrix to form dislocation loops and helices. It was difficult to resolve δ' particles at this stage. Al_3Zr (β') particles were also difficult

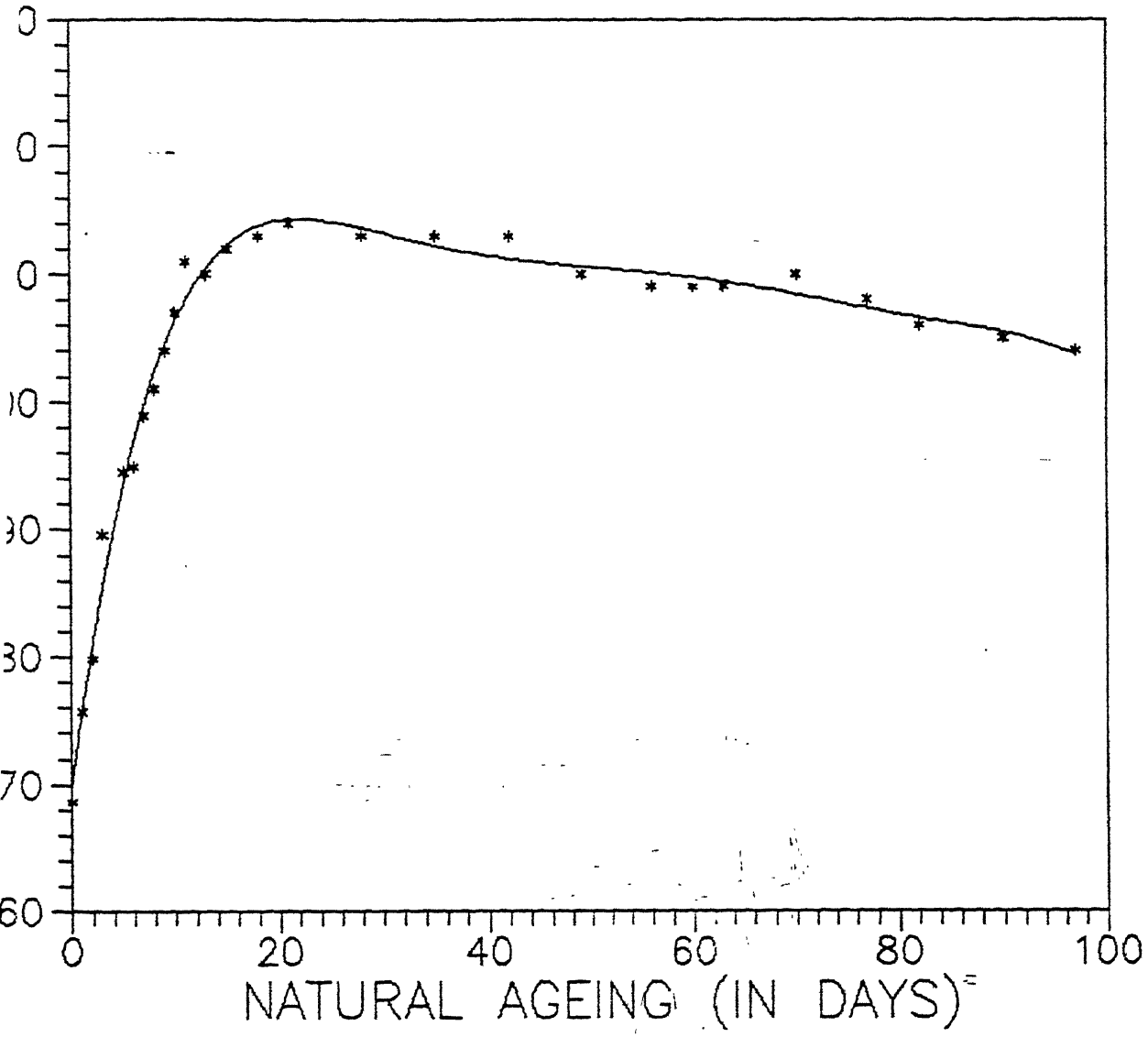

2 NATURAL AGEING RESPONSE OF AS QUENCHED MATERIAL

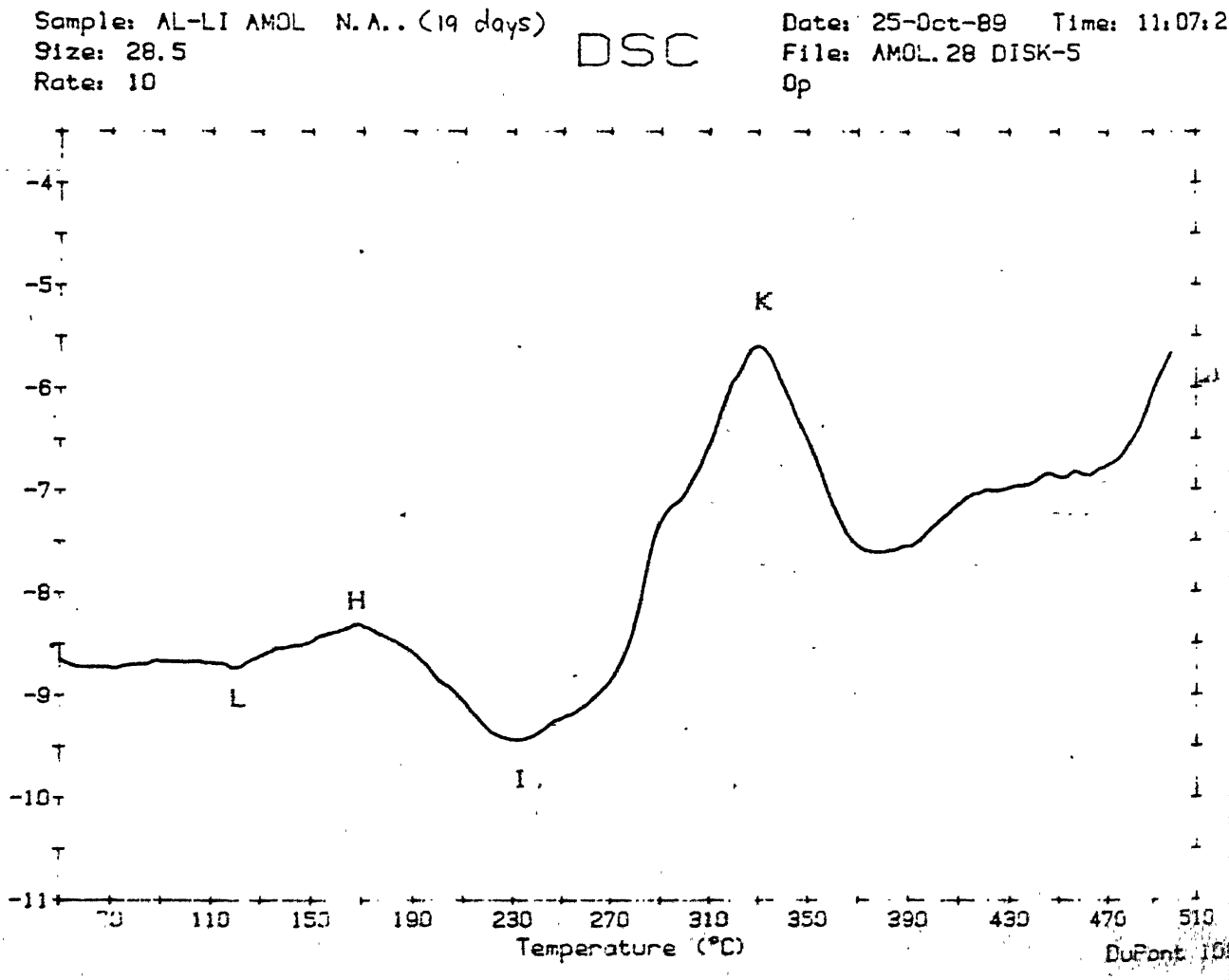

Fig. 23 : DSC thermogram of 19 days naturally aged sample.

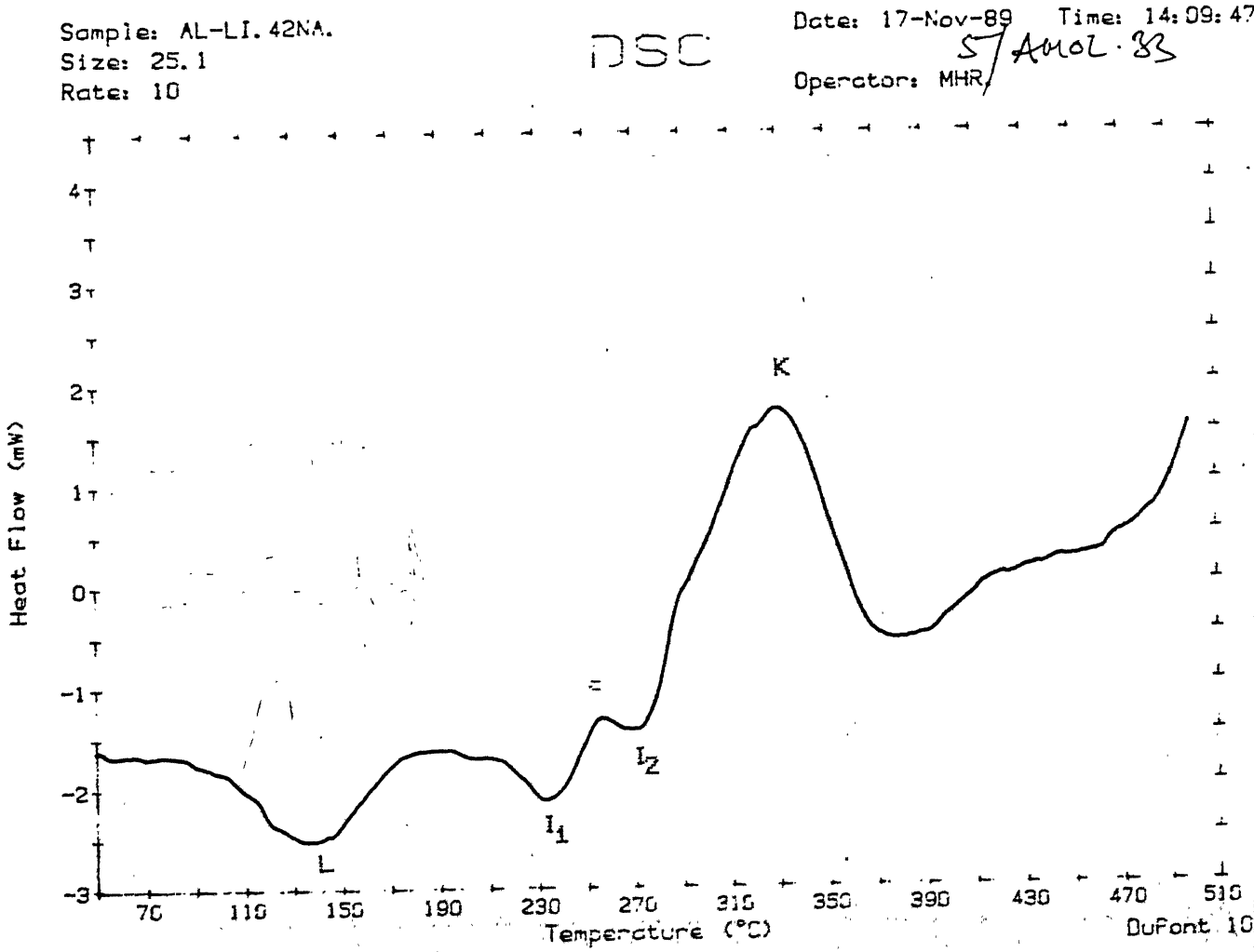

Fig. 24 : DSC thermogram of 42 days naturally aged sample.

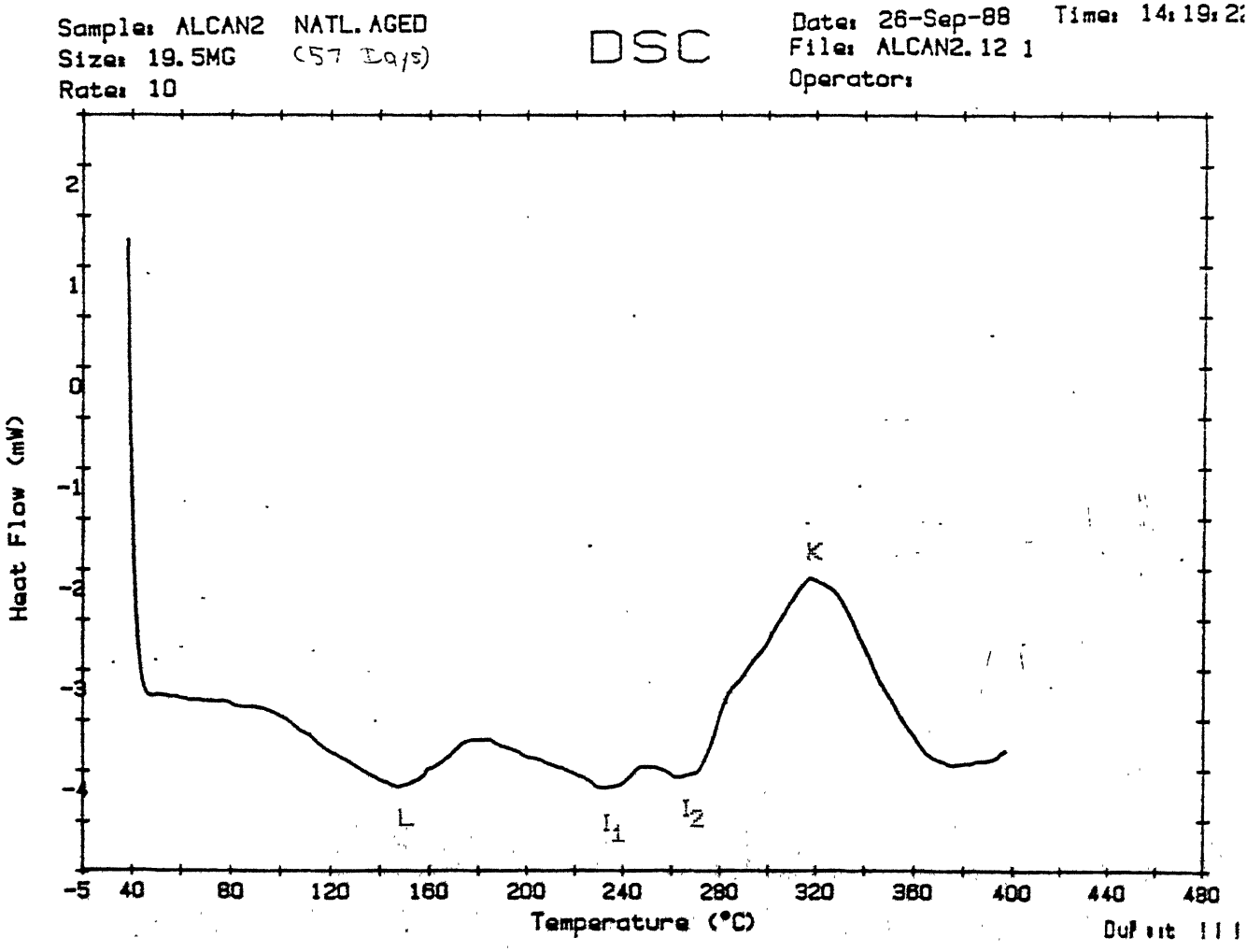

Fig. 25 : DSC thermogram of 57 days naturally aged sample.

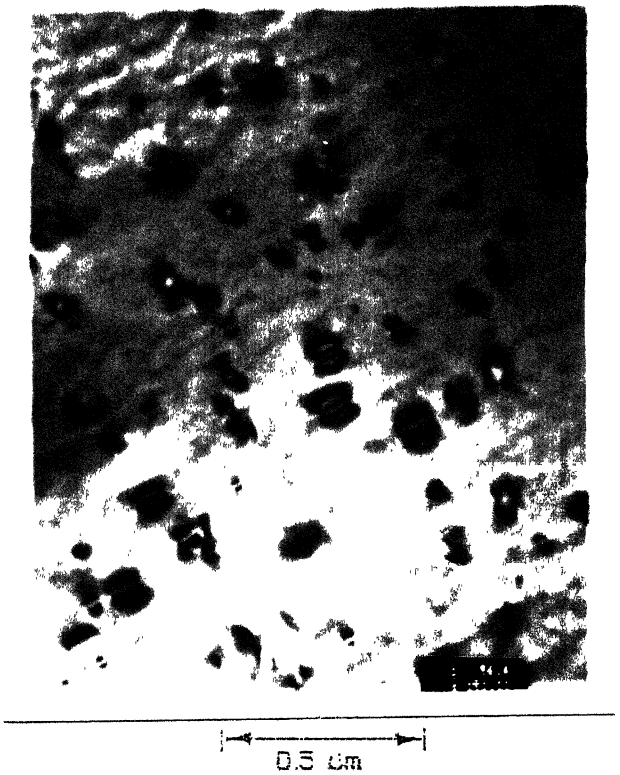

Fig. 26 : Dislocation structure in 57 days naturally aged sample

Fig. 27 : Dislocation structure in 57 days naturally aged sample

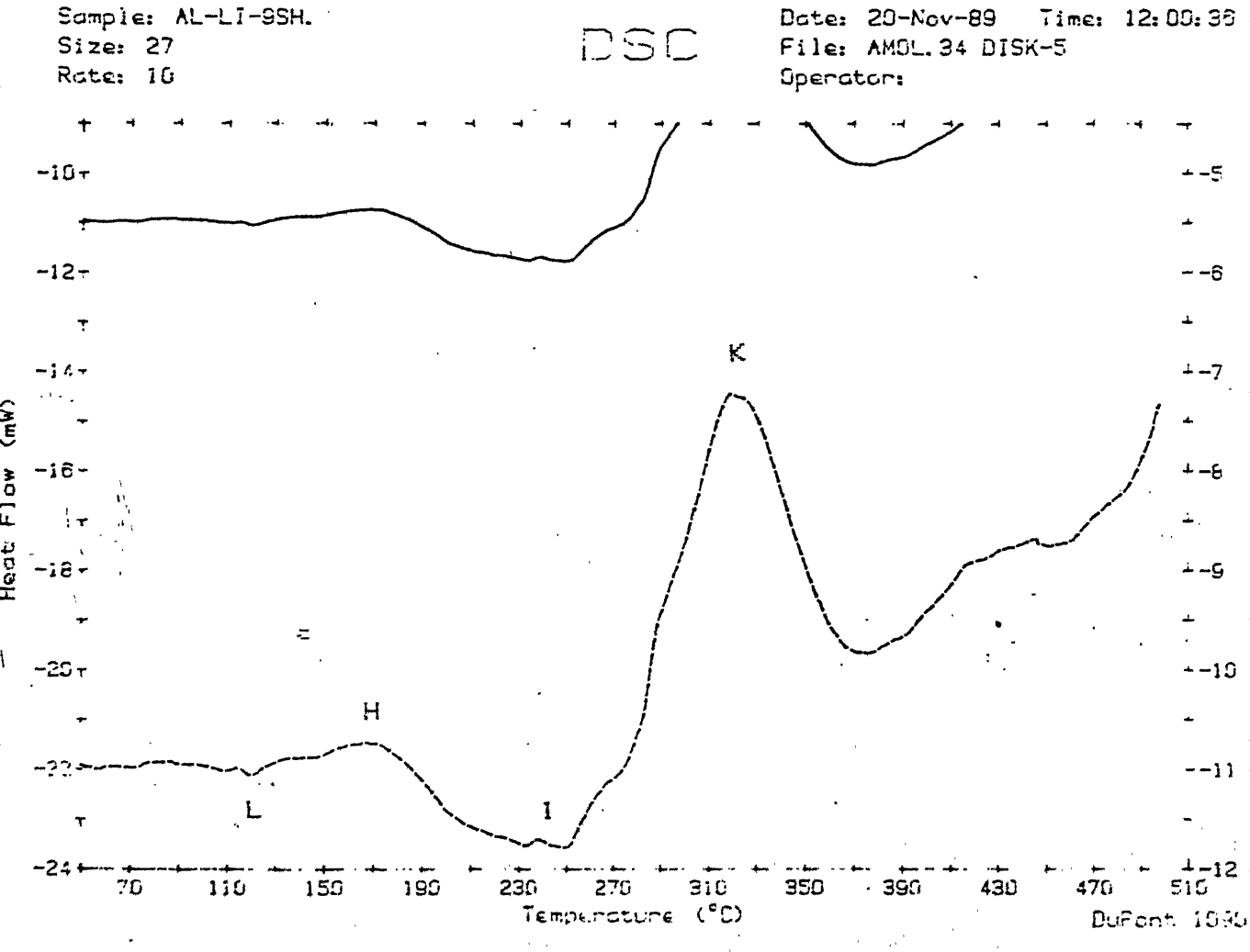

Fig. 29 : DSC thermogram of slowly heated room temperature to 190°C sample

to identify in the bright field image, due to weak contrast between the matrix and (β') particles. But, in Fig. 26 some of the features exhibiting coffee seed contrast could be β' particles.

4.3.2 : Slow Heating

The as quenched sample was heated from room temperature to 190°C with 10°C/hour heating rate. The sample was taken out as soon as 190°C was reached. The hardness was 132 VPN.

Thermal analysis was done within 1 hour and the result is presented in Fig. 28. There is a faint suggestion of endothermic peak (L) at 120°C similar to that observed in the as received (Fig. 14) and 19 days naturally aged (Fig. 23) samples. An exotherm at 170°C (H) is similar to that observed in the as received sample. It is clearly evident that the δ' formation is not complete during this slow heating. The endotherm (I) peak is extended upto 250°C, which is δ' dissolution. It can be concluded that the degree of ageing in this case is in between the naturally aged and the peak aged conditions. Neither δ' formation nor Al-Li G.P. zone replacement is complete during slow heating. The prominent peak present at 315°C (K) is of S and δ precipitation.

Results of the all DSC thermograms presented in this chapter are summarised in Table VII. All the similar type of peaks present in all the six thermograms occurs around the same temperature range.

Table VII on next page.

Table VII : DSC Results

Fig. No.	Condition	Results
14	As received	i) Endotherm at 120°C (L): Al-Li G.P. zone dissolution ii) Exotherm at 170°C (H) : δ' formation iii) Endotherm at 230°C (I) : δ' dissolution iv) Exotherm at 330°C (K) : δ and S formation
18	As quenched	i) Endotherm at 100°C (L) : Al-Cu-Mg G.P. zone formation ii) Exotherm at 170°C (H) : δ' formation iii) Endotherms at 230°C and 270°C (I_1 and I_2) : δ' dissolution iv) Exotherm at 320°C (K) : δ and S formation
23	19 days naturally aged	i) Endotherm at 120°C (L): Al-Li G.P. zone dissolution ii) Exotherm at 170°C (H) : δ' formation iii) Endotherm at 230°C (I) : δ' dissolution iv) Exotherm at 330°C (K) : δ and S formation
24	42 days naturally aged	i) Endotherm at 135°C (L): Al-Li G.P. zone dissolution ii) Endotherms at 230°C and 270°C (I_1 and I_2) : δ' dissolution iii) Exotherm at 330°C (K) : δ and S formation
25	57 days naturally aged	i) Endotherm at 150°C (L): Al-Li G.P. zone dissolution ii) Endotherms at 235°C and 270°C (I_1 and I_2) : δ' dissolution iii) Exotherm at 320°C (K) : δ and S formation
28	Slowly heated to 190°C	i) Endotherm at 120°C (L): Al-Li G.P. zone dissolution ii) Exotherm at 170°C (H) : δ' formation iii) Endotherm at 230°C to 250°C (I) : δ' dissolution iv) Exotherm at 320°C (K) : δ and S formation

4.3.3 : Low Temperature Ageing

The low temperature ageing response at 50°C and 75°C is summarised in Fig. 29. The peak hardness (109 VPN) is reached after 144 hours during the 50°C ageing treatment. The peak hardness for 75°C ageing occurs over a range between 40 and 115 (113 VPN) hours. The main object to study low temperature ageing was to find a shorter time equivalent to natural ageing. The ageing period of 40 to 115 hours at 75°C or 144 hours at 50°C is resonably shorter than 12 days natural ageing period, when compared on the basis of hardness values. Selected samples were subjected to high temperature ageing at 190°C, 20 hours. Hardness results are summarised in Table VIII.

Table VIII : Hardness data of low temperature aged + 190°C aged samples.

Sample History	*Hardness (VPN)*
1) 48 hours at 50°C + 190°C (20 hours)	138
2) 144 hours at 50°C + 190°C (20 hours)	140
3) 45 hours at 75°C + 190oC (20 hours)	138
4) 115 hours at 75°C + 190°C (20 hours)	113

The hardness values of 50°C + 190°C, 20 hours treatment indicates that the samples have just crossed peak-ageing (as a result of additional diffusion occuring at 50°C). The 75°C preageing has similar effect. It is possible that there was a loss of vacancies released due to δ' precipitation to the subgrain boundaries during prolonged low temperature ageing. This would result in lower free vacancy concentration in the matrix and less promotion of S phase. Thus, high temperature ageing (190°C) with shorter time (less than 20 hours) should be studied to achieve peak-ageing in the low temperature processed samples.

4.4 : Artificial Ageing At Different Temperatures

The response to artificial ageing at 190°C is demonstrated in Fig. 30. The three curves pertain to different pre-ageing conditions : as quenched, 12 days naturally aged, and slowly heated from room temperature to 190°C. The peak in ageing curve occurs at around 20 hours in each case. The peak hardness of naturally aged and slowly heated samples is slightly more. The onset of overageing is inhibited to some extent in naturally aged samples. In the overaged condition naturally aged sample shows more hardness.

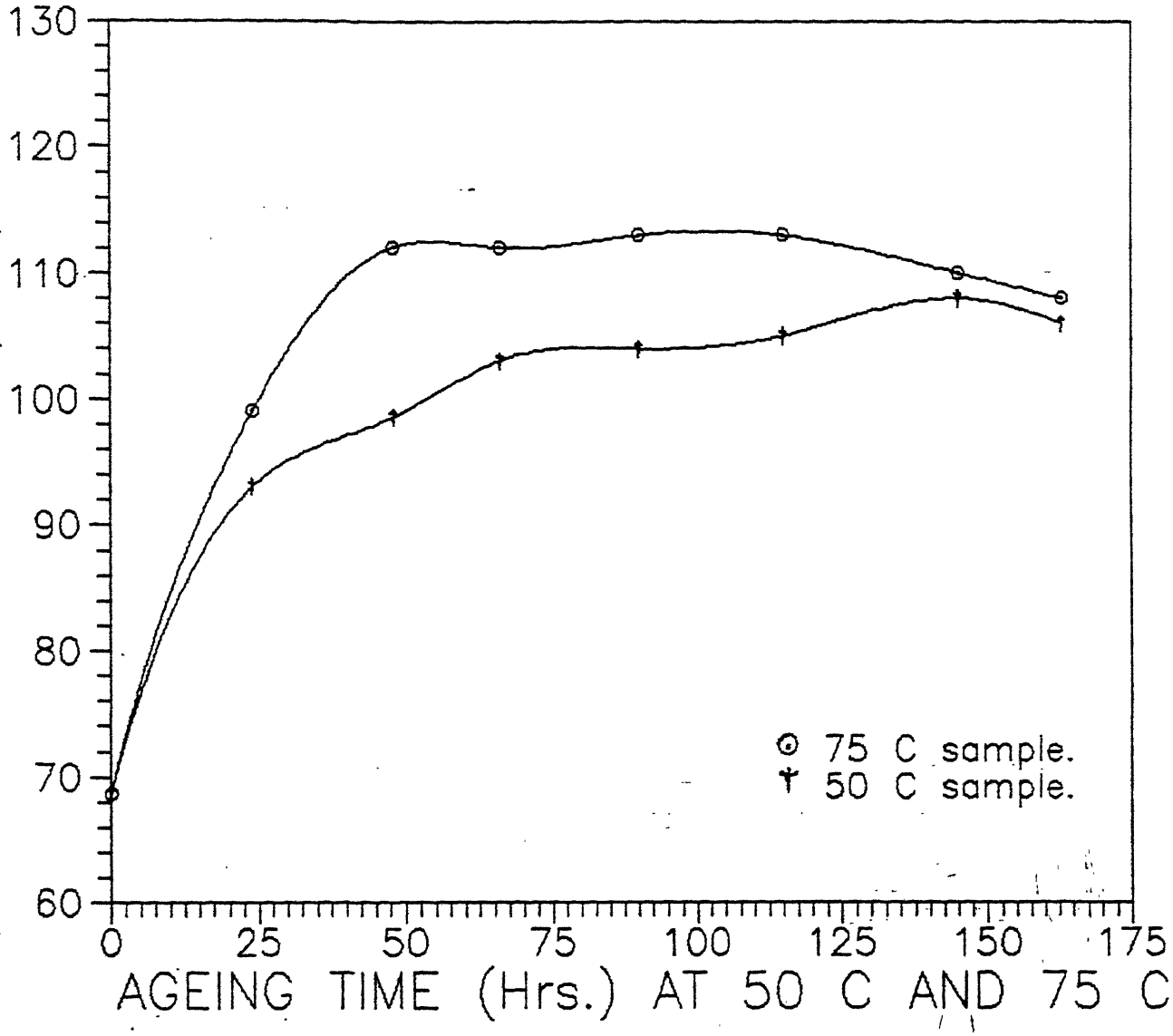

Fig.29 LOW TEMPERATURE AGEING CURVES.

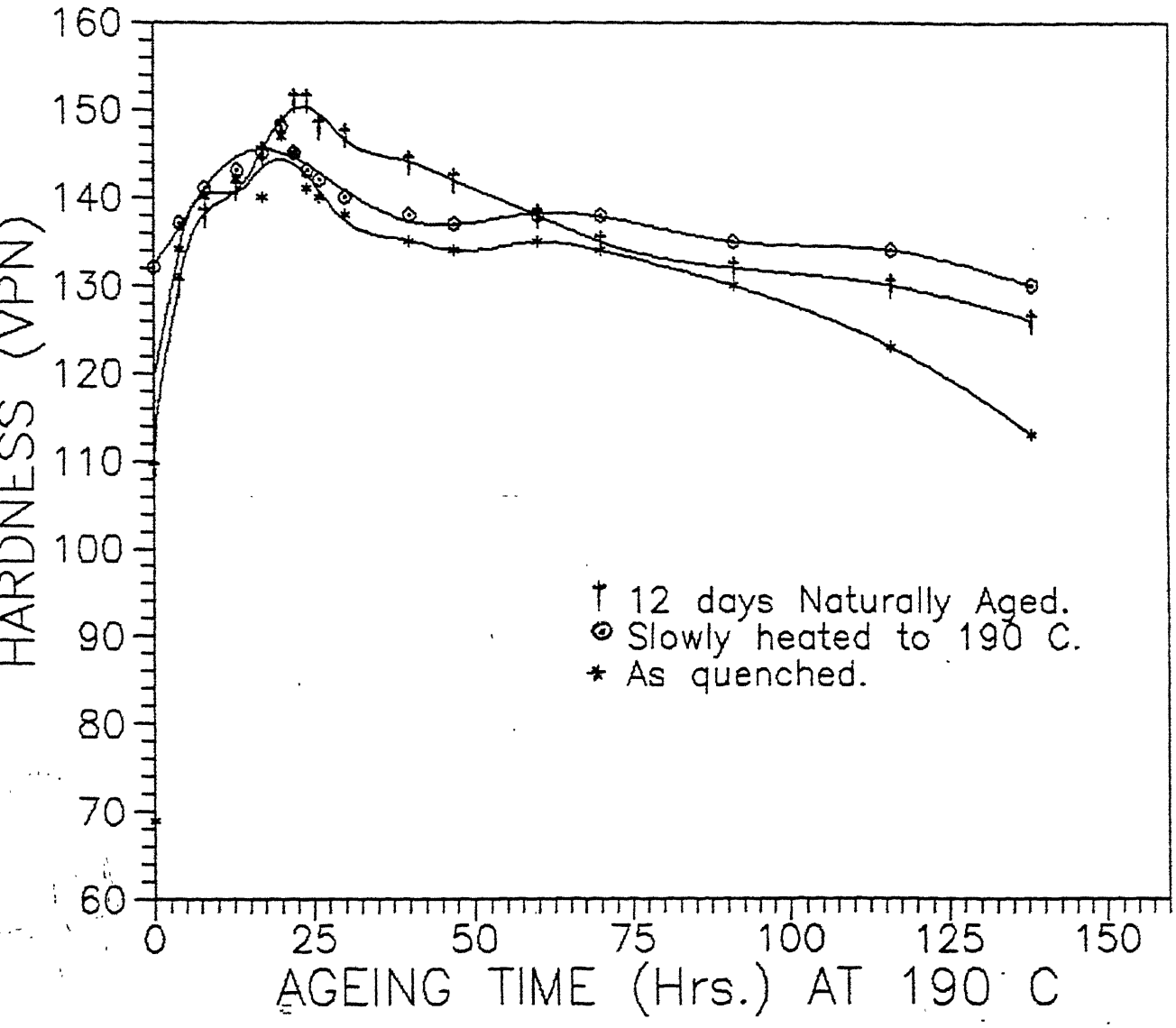

Fig.30 THERMAL AGEING RESPONSE AT 190 C.

Four different artificial ageing treatments with equivalent Li diffusion distances (160^0C-196 hrs., 170^0C-89 hrs., 180^0C-42 hrs., 190^0C-20 hrs.) were employed to the samples of different pre-ageing histories as mentioned above. The hardness of these samples (VPN) after high temperature ageing is given in Table IX. The abbreviations A.A., N.A., S.H., R.T. used in this chapter mean as following :

A.A. : Artificial Ageing; N.A.: Natural Ageing;

S.H. : Slowly Heated; R.T. : Room Temperature.

Table IX : Hardness data at four different temperatures with different pre-ageing history.

	Hardness in VPN			
Condition	160^0C	170^0C	180^0C	190^0C
a) A.A.	156	151	143	147
b) 12 Days N.A. + A.A.	159	147	142	148
c) 42 Days N.A. + A.A.	157	148	147	145
d) S.H. From R.T. + A.A.	160	150	151	148
e) S.H. From R.T.	122	124	127	132

The hardnesses for 160^0C ageing are comparetively higher than for ageing at 190^0C and this was expected on the basis of greater driving force for nucleation of δ' at 160^0C. The higher hardness of slowly heated samples to the final ageing temperature (d) lot in table IX) is due to additional time at elevated temperature before the final ageing temperature is reached. It increases the size (diameter) of δ' at that temperature, which improves strength level.

4.5 : Effects Of Thermal Treatments On The Microstructure

4.5.1 : δ' Distribution And PFZ

The distribution of δ' precipitates was studied for two different artificial ageing temperatures (160^0C and 190^0C), with different preageing histories. All the micrographs are taken in dark field. The results are presented in Figs. 31-38. The δ' phase is uniformly distributed throughout the matrix in all the conditions. δ' is finer and more densely populated in 160^0C case than in 190^0C , as would be expected due to greater driving force for δ' nucleation at 160^0C . It was not possible to estimate volume fraction of δ' because of difficulty to measure foil thickness accurately. The average δ' size was measured from the micrographs. The

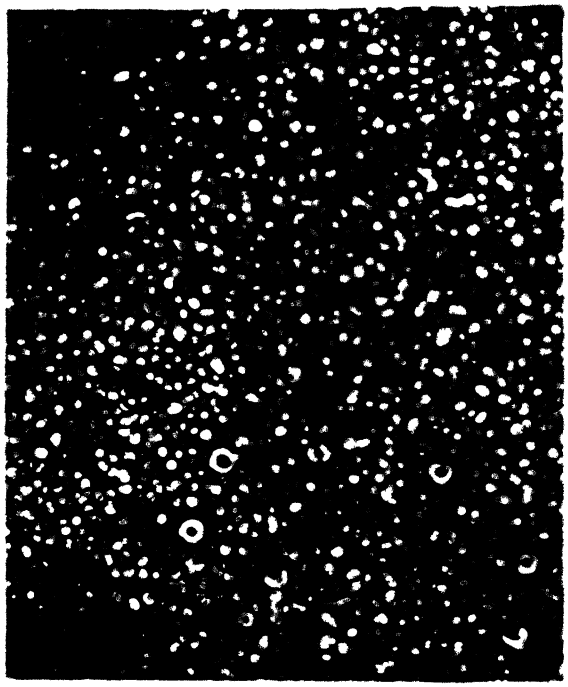

Fig. 31 : δ' micrograph of 160°C, 198 hrs. AA sample

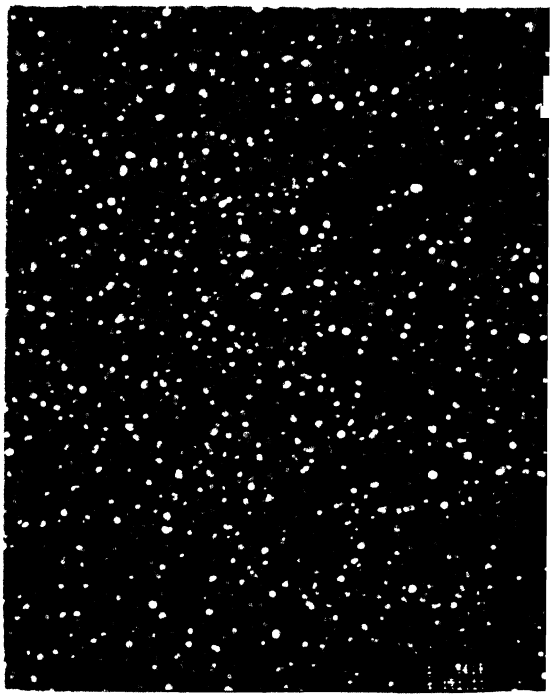

Fig. 32 : δ' micrograph of 12 days N.A + 160 AA sample.

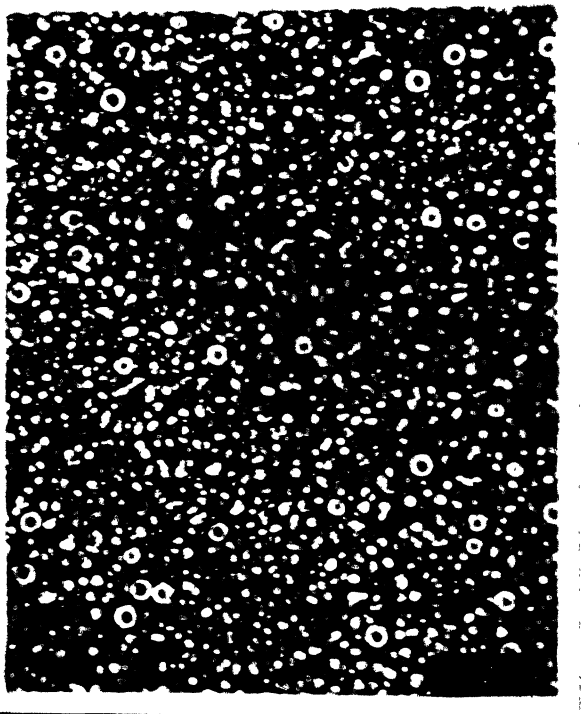

Fig. 33 : δ' micrograph of 42 days N.A + 160 AA sample.

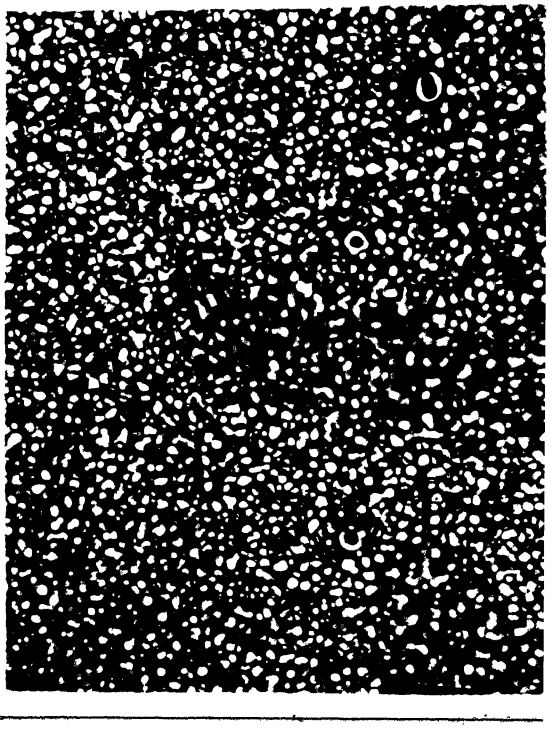

Fig. 34 : δ' micrograph of slowly heated + 160 AA sample.

Fig. 35 : δ' micrograph of 190°C, 20 hrs. AA sample

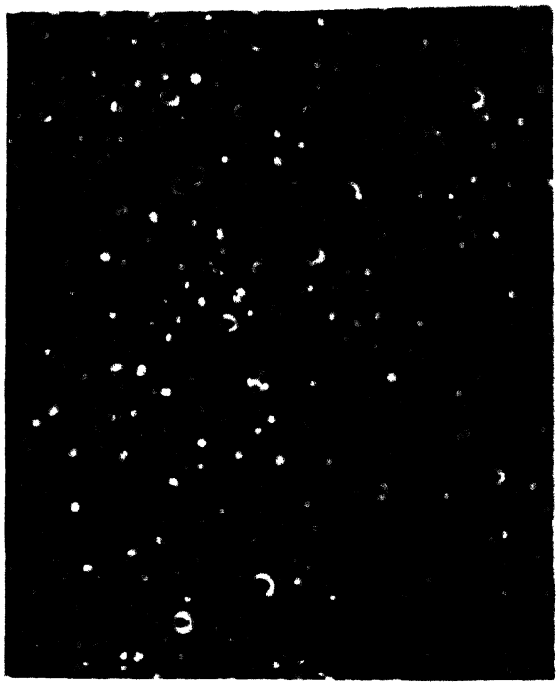

Fig. 36 : δ' micrograph of 12 days N.A + 190 AA sample.

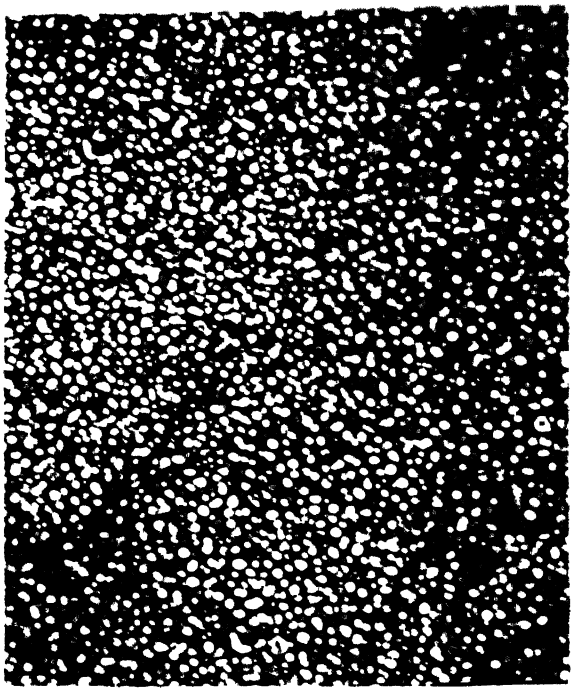

Fig. 37 : δ' micrograph of 42 days N.A + 190 AA sample.

Fig. 38 : δ' micrograph of slowly heated + 190 AA sample.

Fig. 39 : δ' PFZ micrograph of 160°C, 198 hrs. AA sample

Fig. 40 : δ' PFZ micrograph of 12 days N.A + 160 AA

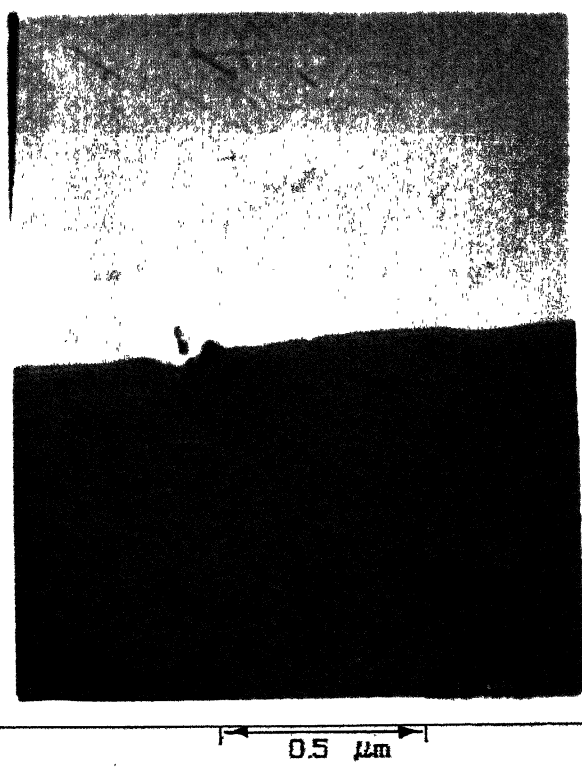

Fig. 41 : δ' PFZ micrograph of 42 days N.A + 160 AA sample

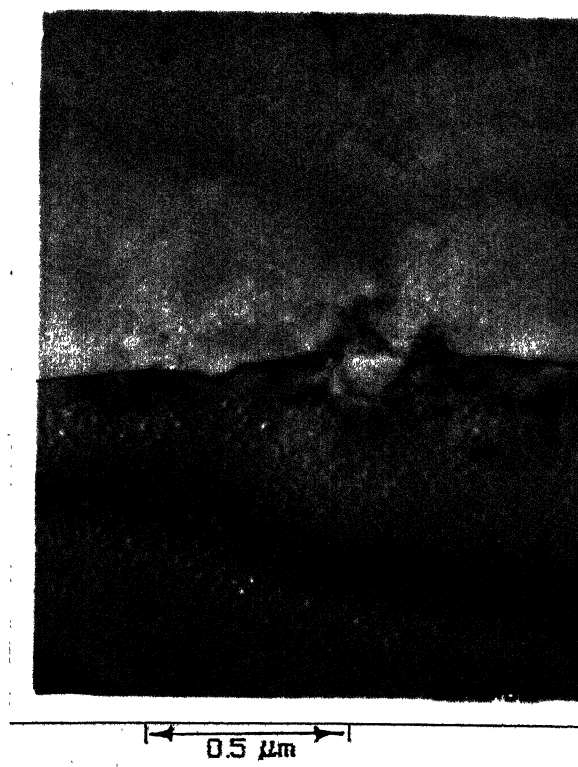

Fig. 42 : δ' PFZ micrograph of slowly heated + 160 AA sample.

Fig. 43 : δ' PFZ micrograph of 190°C, 20 hrs. AA sample

Fig. 44 : δ' PFZ micrograph of 12 days N.A + 190 AA

Fig. 45 : δ' PFZ micrograph of 42 days N.A + 190 AA sample

Fig. 46 : δ' PFZ micrograph of slowly heated + 190 AA sample.

results are presented in table X. The abbreviations in the table X mean same as in table IX.

Table X : Average δ' size

Fig. No.	Condition	δ' dia. in nm.
31	160 A.A.	24
32	12 days N.A. + 160 A.A.	17
33	42 days N.A. + 160 A.A.	21
34	S.H. from R.T.to 160 + 160 A.A.	22
35	190 A.A.	30
36	12 days N.A. + 190 A.A.	25
37	42 days N.A. + 190 A.A.	31
38	S.H. from R.T.to 190 + 190 A.A.	36

Bull's eye structure (δ' on the $Al_3Zr(\alpha')$ particles) was observed in all the ageing conditions (Figs. 31, 33, 35 and 36 clearly show this feature). The distribution of Al_3Zr (β') particles, which depends upon the processing history, was found to be non-uniform.

δ' PFZ

The δ' PFZ micrographs corresponding to ageing conditions similar to those of Figs. 31-38 are presented in Figs. 39-46. The PFZ width in the unrecrystallised Al-Li alloys such as the present one is quite non-uniform and seems to depend upon orientation with respect to the rolling plane. PFZ widths were therefore calculated from foils oriented parallel to the L-T plane of the rolled plate, and are summerised in table XI. Care was taken to orient the foil so as to observe true width of the PFZ.

Table XI : δ' PFZ Width

Fig. No.	Condition	Half width of the PFZ (μm).
39	160 A.A.	0.135
40	12 days N.A. + 160 A.A.	0.083
41	42 days N.A. + 160 A.A.	0.076
42	S.H. from R.T.to 160 + 160 A.A.	0.069
43	190 A.A.	0.129
44	12 days N.A. + 190 A.A.	0.180*
45	42 days N.A. + 190 A.A.	0.073
46	S.H. from R.T.to 190 + 190 A.A.	0.163*

Samples which received preageing treatments seem to have narrower δ'-PFZ's (with a few exceptions *), possibly because of greater nucleation of δ' taking place. In general, it seems that PFZ widths for 160°C and 190°C ageing are comparable. It is expected to be so, as both the treatment times were estimated on the basis of equal Li diffusion distances.

4.5.2 : S Distribution And PFZ

S distribution in samples aged at 160°C and 190°C are presented in Figs. 47-54. S phase in case of 190°C ageing seems to be coarser and the volume fraction is also slightly more than in case of 160°C ageing. The lower density of S phase corresponding to 160°C treatment could be because of lower diffusivity of Cu and Mg at 160°C .

Natural ageing aids precipitation of S phase in the matrix. Dislocation loops and helices developed in the naturally aged samples acts as nucleation sites for S phase during subsequent artificial ageing. 42 days of natural ageing in both cases seems to be attractive for S nucleation, whereas, the density of vacancy defects generated during 12 days natural ageing is not enough to accelarate heterogeneous S phase distribution during subsequent artificial ageing at 160°C (the diffusivity of the solute atoms at 160°C is not enough).

Slow heating to the final ageing temperature was reported (for an 8091 Al-Li alloy) to give widespread precipitation of S in the matrix [76]. It is assumed that during slow heating release of vacancies occur in a controlled manner (as Li precipitates to form δ'), which is responsible for aiding S precipitation in the microstructure. In the present case, slow heating upto 160°C did not give such results. Slow heating to 160°C might not be creating sufficient concentration of free vacancies, which will accelarate S nucleation in the matrix. Whereas, slow heating to 190°C shows similar S distribution as naturally aged samples. It should be noted that in case of 8091 alloy, Cu and Mg supersaturation of the matrix is more than in case of 8090 alloy, providing greater thermodynamic driving force for S precipitation.

To conclude, in 160°C artificial ageing practice prolonged natural ageing (atleast 42 days) is essential for heterogeneous nucleation of S phase. In 190°C artificial ageing practice natural ageing can be replaced by slow heating.

Fig. 47 : S distribution in 160^{0}C, 198 hrs. AA sample

Fig. 48 : S distribution in 12 days NA + 160 AA sample.

Fig. 49 : S distribution in 42 days NA + 160 AA sample

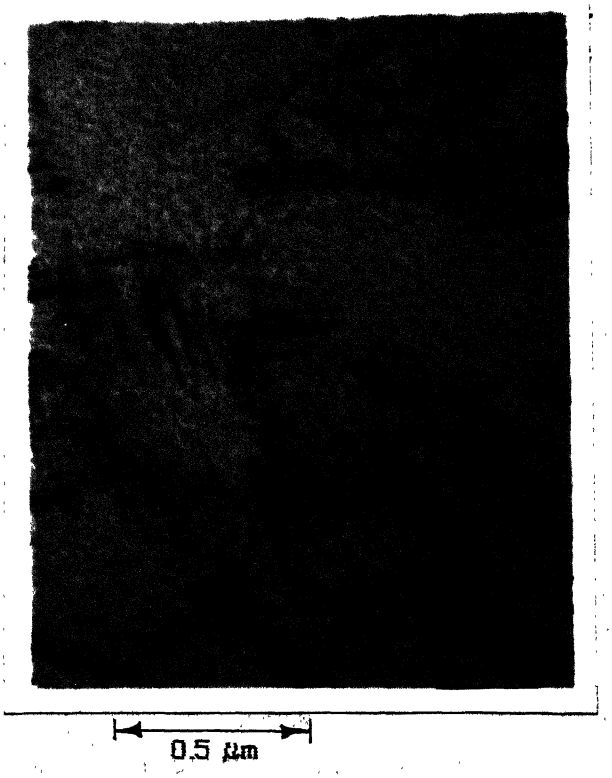

Fig. 50 : S distribution in slowly heated + 160 AA sample.

Fig. 51 : S distribution in 190°C, 20 hrs. AA sample

Fig. 52 : S distribution in 12 days NA + 190 AA sample.

Fig. 53 : S distribution in 42 days N.A + 190 AA sample.

Fig. 54 : S distribution in slowly heated + 190 AA sample.

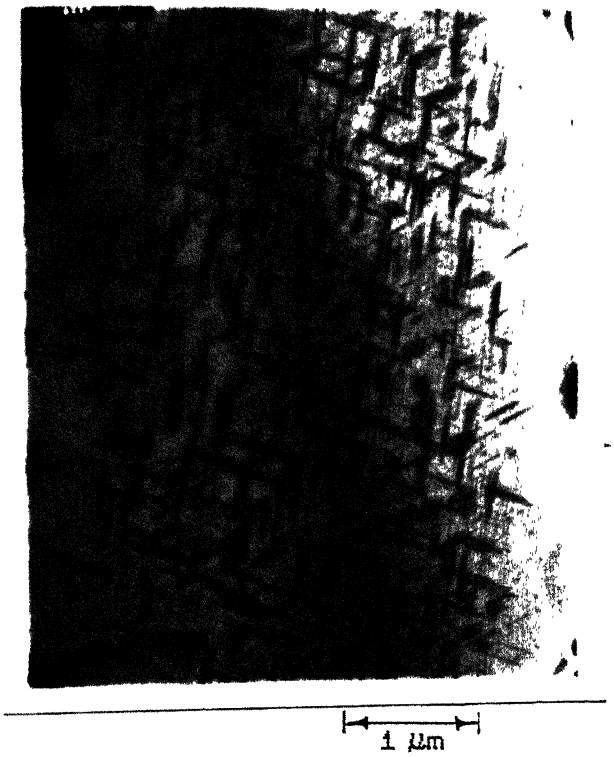

Fig. 55 : S PFZ in 42 days naturally aged + 160 AA sample.

Fig. 56 : S PFZ in 42 days naturally aged + 190 AA sample.

Fig. 57 : S PFZ in 42 days naturally aged + 190°C + 190 AA sample.

S PFZ

Since, 42 days natural ageing or slow heating to artificial ageing temperature are the favourable conditions for the S precipitation, PFZs were observed at some high angle grain boundaries in few ageing condition. The mechanism is probably same as δ' PFZ formation (solute depletion) along the high angle grain boundaries. The PFZ width was measured and the results are summarised in Table XII.

Table XII : S PFZ Width

Fig. No.	Description	Half PFZ Width In μm.
55	42 days N.A. + 160 A.A.	0.58
56	42 days N.A. + 190 A.A.	0.58-0.94
57	S.H. from R.T.to 190 + 190 A.A.	0.35-0.58

The S PFZs reported in the literature are summarised in Chapter II [76,97]. The results obtained in the present investigation are comparable to them. S PFZ is deleterious to the mechanical properties, and further attempts may be made to reduce S-PFZ (stretching is shown to be one such alternatives [63]).

4.5.3 : T_1 Distribution

In 190^{0}C directly artificially aged Fig. 58, 12 days naturally aged and artificially aged at 190^{0}C Fig. 59 and slowly heated to 190^{0}C and artificially aged Fig. 60 samples, T_1 was observed at some places. However, its volume fraction was very low. This could be due to the favourable conditions for S phase formation in this alloy, and consequently less availability of Cu for T_1 precipitation. In this regard, the Cu:Li and Cu:Mg ratios are very important. In general, from the point of view of mechanical properties, T_1 phase is less attractive than S phase.

4.6 : General Discussion

The results of the present investigation (δ' size, δ' PFZ width, S PFZ, and presence of T_1 and hardness measurements) presented in the earlier sections are summarised in Table XIII.

P.T.O.

Fig. 58 T_1 in 190°C AA sample.

Fig. 59 T_1 in 12 days NA + 190 AA. sample.

Fig. 60 T_1 in slowly heated to 190°C + 190 AA. sample.

Table XIII : Summary of microstructural features and hardness measurements for various treatments

Condition	δ' dia. in nm	δ' PFZ in μm	Hardness (VPN)	S PFZ in μm	T_1
As received	15	0.017	165	-	-
160 A A	24	0.135	156	-	-
12 days N A +160 A A.	17	0.083	159	-	-
42 days N A +160 A A.	21	0.076	157	0.58	-
S H from R T to 160 + 160 A A.	22	0.069	160	-	-
190 A A.	30	0.129	147	-	Y
12 days N A +190 A A	25	0.18	148	-	Y
42 days N A +190 A A	35	0.073	145	0.58-0.94	-
S H from R T to 190 + 190 A A.	36	0.163	148	0.35-0.58	Y

One important point to note is that all the hardness values reported are less than that of the as-received material (165 VPN). Artificial ageing at 160°C following natural ageing or slow heating yields higher hardness values than those obtained after the 190°C heat treatment.

The width of the δ' PFZ corresponding to the 160°C treatment is narrower than what is obtained after the 190°C ageing treatment. Since the choice of the optimum heat treatment condition depends on the peak hardness value as well as the width of δ'-PFZ, it is clear from table XIII, that the choice of 160°C ageing treatment is superior to that at 190°C. The former, as is clearly pointed out in the literature, would also have less grain boundary precipitates - an additional desirable feature. Slow heating to 160°C gives the best combination of hardness and δ' PFZ. It would be desirable to check whether the variation in the heating rate to 160°C (say 20°C/hour instead of 10°C/hour) would still give rise to the same beneficial effect. This would result in a lower time for the completion of the entire heat treatment operation.

The lower density of S phase in slowly heated to 160°C sample is not satisfactory. As S phase is effective in breaking up coplanar slip (due to δ' shearing); alternative heat treatment to aid S precipitation alongwith lower δ' PFZ width, and higher hardness should be investigated.

CHAPTER V
CONCLUSIONS AND SUGGESTIONS FOR FURTHER WORK

1) The 8090-T851 alloy received from ALCAN (U.K.) was shown to be in an underaged condition (with the help of DSC and microstructure comparisons).

2) In the as-quenched sample dislocation loops and superdislocations were present. It was not possible to observe δ' or β' in the matrix.

3) The DSC study of 19 days naturally aged sample indicates that δ' growth is incomplete

4) DSC study of 42 days naturally aged sample showed Al-Li G.P. zone dissolution peak

5) Natural ageing releases bound vacancies (as δ' grows) which precipitate as dislocation loops and helices. This behaviour was spontaneously observed in 57 days naturally aged sample.

6) The onset of overageing occurs after 77 days natural ageing.

7) The volume fraction of δ' and width of δ'-PFZ appeared similar in all cases, with slightly finer δ' size for 160°C ageing condition.

8) Distribution of S phase could be improved by incorporating preageing treatments such as natural ageing and slow heating to the final ageing temperature.

9) PFZ width along the high angle grain boundary was slightly narrower in naturally aged sample.

10) The slow heating does not have much effect on S precipitation in ageing at 160°C, whereas the natural ageing period can be replaced in ageing at 190°C.

11) S PFZ was observed in 42 days naturally aged sample + artificially aged sample as well as in slowly heated to the final ageing temperature + artificial aged at 190°C.

12) T_1 was observed in small quantity, when the samples were aged at 190°C.

P.T.O.

Suggestions for further work

1) High resolution microscopy is required to differentiate δ' and G.P. zones in naturally aged samples

2) It is necessary to investigate onset of overageing, which is observed after 77 days natural ageing. To date, such results have not been reported.

3) S precipitation is strongly dependent on dislocation structure and vacancy defects present in the matrix. The study concerning solute-vacancy interactions should be performed.

4) Natural ageing prior to artificial ageing has shown lesser δ' PFZ width in the matrix. Effect of natural ageing at low temperature ageing ($160^{0}C$ or $170^{0}C$) on PFZ width and grain boundary precipitate should be investigated.

5) Slow heating to the final ageing temperature should be applied with the different heating rate, to study the effect on formation of S and δ' PFZ .

ACKNOWLEDGMENT

I take this opportunity to express my gratitude to the Scientists in DMRL, Hyderabad and my Professors and friends in IIT Kanpur who guided and helped me in this thesis. Prof.T. R. Ramachandran helped me to select the topic and gave the initial impetus for this work. I sincerely thank Prof. T. R. Ramachandran for his guidance and encouragement throughout the course of the present work. The experimental work has been carried out at D.M.R.L.,Hyderabad. Dr. Amol Gokhale, Scientist, DMRL, HYDERABAD has been a continuous source of inspiration and encouragement during the stay at Hyderabad. I am greatly indebted to him for his guidance and support. I am grateful to Prof. G. S. Murthy, whose advice and involvement in the project work helped me a lot.

The Transmission Electron Microscopy was the backbone of the thesis. I thank Mr. K. S. Prasad, Scientist, TEM Group, DMRL, without whose efforts this work could not have been completed. My friends Shripad Ponkshe, Manvendra Bhangui, Sanjay Jain and colleague Avnish Srivastava have always been at my disposal for rendering all kinds of help and assistance with a sense of brotherly affection. The same is most graciously acknowledged.

I am indebted to Scientists in DMRL Dr. C.R. Chakravarty, Dr. D. Banerjee, Dr.(Mrs.) Heena Gokhale, Mr. R.P. Mathur, Mr. M.K. Jain, Mr. Vijay Singh, Miss Smita Shanbag and DESIDOC INCHARGE Mr. Sunil Dhar for their encouragement and help during the course of this research. I would like to express my heart felt gratitude to them.

I am deeply indebted to my mother, sister and all my close relatives for their best wishes and spiritual support. My friends are too numerous to be listed and acknowledged. I can not mention all of them. But some of them have loomed so large that they must be acknowledged. The dramatics and trekking group of my friends Sandeep Kulkarni, Prashant Rane, Sandeep Nawathe, and Abhay Ranade culturally enriched the last two years. Chandra Shekhar, Sridhar, V.S.Rana and Satish Gupta contributed greatly towards making my stay at DMRL, Hyderabad intellectually fruitful one.

Last but not the least, I acknowledge the assistance of all my batchmates and all those whose involvement made the present work possible.

Nitin V. Joshi.

REFERENCES

1] T.R. Pritchett, Light Metal Age, August, 1986, pp. 10-14.

2] K. K. Sankaran, S. M. L. Sastry and J. E. O'Neal, See 30, pp. 189.

3] P. S. Gilman and J. S. Benjamin, Annual Review of Material Science, 13, Annual Reviews, Inc., Palo Alto, CA, 1983, p.273

4] F. Beniere, M. Chemla, M. Aucouturier, P. Lacombe, and C. Roques., Corrosion-Nace, Vol. 24, April 1968, pp 83 - 89.

5] D. B. Williams, and J. W. Edington, J.W., Met. Sci., Vol.9, 1975, pp.529-532.

6] P.J. Gregson and H.M. Flower, Acta Met., 33, 1985, pp. 527.

7] Report on Installation of Al-Li ingot casting facilities, DMRL, Hyderabad, Jan 1989.

8] F. W. Gayle, "Aluminium - Lithium Alloys I ", edited by T.H. Sanders, Jr., and E.A.Stark, Jr., (AIME, New York, 1981) , pp. 119.

9] S. F. Baumann and D. B. Williams, Aluminium-Litthium Alloys II, ed. T. H. Sanders Jr. and E.A.Starke Jr., TMS-AIME, Warrendale, Pa., 1983, p. 17.

10] Ola Jensrud and Nils Ryum, Mat. Sci. and Engg., 64 (1984), 229.

11] B. Noble, S. J. Harris and K. Dinsdale, Journal of Materials Science, 17 (1982), 461.

12] K. K. Sankaran, S. M. L. Sastry and J. E. O'Neal, See 8, pp. 189.

13] K. Dinsdale, S.J. Harris and B. Noble, See 8, p. 101.

14] N. C. Parson and T. Sheppard, See 9, p. 53.

15] P. Niskanen, T.H. Sanders, Jr., J. G. Rinker and M. Marek, Corrosion Science, 22 (1982), 283.

16] G. E. Thompson and B. Noble, J. Inst. Metals, 101 (1973), 111.

17] I. G. Palmer, R. E. Lewis D. D. Crooks, High Strength Powder Metallurgy Aluminium Alloys, TMS-AIME, Warrendale (1982), p. 369.

18] S. J. Harris, B. Noble and K. Dinsdale, See 9, p. 219.

19] W. E. Quist, G. H. Narayanan and A. L. Wingert, , see 9, pp. 313.

20] T. H. Sanders Jr., and E. A. Starke, Jr., See 9, p. 1.

21] P. Niskanen, T.H. Sanders, Jr., G. Rinker, M. Marek, Corr. Sci., 22 (1982), pp 461.

22] S.J.Harris, B.Noble and K. Dinsdale, Al-Li Conf. IV, J. De Physique, Colloque 3(9), Tome 48, G. Champier, B.Dobost, D.Miannay, L.Sabetay (Eds.), 1987, pp. C3-415.

23] K.K. Sankaran, S.M.L. Sastry, and J.E. O'Neil, see 8, pp.190-203.

24] F. W.Gayle, as 8, pp. 119-139.

25] R.C.A. Pratt, P. Tsakiropoulos, H. Jones, R.W. Gardiner, and J.E. Restall, as 22, pp. C3 341.

26] W.S. Miller, A.J. Cornish, A.O. Titchener, and D.A. Bennett, as 9, pp 335.

27] T.S. Srivatsan, J. Mat. Sci. Letters, 6, 948, 1987.

28] F. W. Gayle, N. F. Levoy and J. B. Vendersande, J. Met. 39 (1987), p.33

29] S. M. L. Sastry and J. E. O'Neal, as 9, p. 79.

30] P. Lovise Makin and Brian Ralph, J. Mater. Sci., 19 (1984), 3835.

31] C. Sigli and J. M. Sanchez, Acta Metall., 34 (1986), 1021.

32] A. J. McAlister, Bull. Alloy Phase Diagrams, 3(2), (1982), 177.

33] W.R.D. Jones and P.P.Das, J. Inst. Met, 87(1958-59), 338

34] Williams D.B., and Edington J.W., Met. Sci. J., Vol. 5, 1975, pp. 529-532.

35] Williams D.B., Al-Li Conf. V., Univ. Of Virginia, May 1989, pp. 551-563.

36] R. C. Dorward, Met. Trans. 19A, June 1988.

37] The Statistician, by Quant Systems, Charleston, SC, 1981.

38] S. Ranganathan and Alok Singh, Proc. of the seminar on science and tech. of Al-Li alloys., Bangalore, pp 37

39] Nozato R., and Nakai G., Trans. J.I.M., Vol. 18, 1977, pp. 679-689

40] A. K. Mukhopadhyay, C. N. J. Tite, H. M. Flower, P. J. Gregson and F. Sale, See 22, p. 439.

41] Papazian J. M., Sigli C., and Sanchez J.M., Scripta Met., Vol. 20, 1986, pp.201-206.

42] S. Ceresara, A. Giarada, and A. Sanchez, Philos. Mag., 1977, Vol. 35, 97-110.

43] Livet A., and Bloch D., Scripta Metall., Vol. 10, 1985, pp. 1147-1151

44] Spooner S., Williams D. B., and Sung C.M., Aluminium-lithium III, Eds. C. Baker et al., The Inst. Of Metals, London, 1986, pp. 329-336.

45] Balmuth E.S., Scripta Met., Vol. 18, 1984, pp.301-306.

46] Janos Lendvai, Hans-Joachim Gudladt, Wilfried Wunderlich, and Volkmar Gerold, Z. Metallkde.,1989,pp.310-317.

47] P. J. Gregson and H. M. Flower, J. Mat. Sci. Letters, 3, 829 (1984).

48] P. J. Gregson, H. M. Flower, C. N. J. Tite and A. K. Mukhopadhyay, Mat. Sci. Tech., 2, 349, 1986.

49] Al-Li 5 / 721

50] S. Fuzikawa, M. Furukawa, M. Sakauchi and K. Hirano, See 22, pp. 365.

51] P. L. Makin and B. Ralph, J. Met. Sci., 19, 3835 (1984)

23] K.K. Sankaran, S.M.L. Sastry, and J.E. O'Neil, see 8, pp.190-203.

24] F. W.Gayle, as 8, pp. 119-139.

25] R.C.A. Pratt, P. Tsakiropoulos, H. Jones, R.W. Gardiner, and J.E. Restall, as 22, pp. C3 341.

26] W.S. Miller, A.J. Cornish, A.O. Titchener, and D.A. Bennett, as 9, pp 335.

27] T.S. Srivatsan, J. Mat. Sci. Letters, 6, 948, 1987.

28] F. W. Gayle, N. F. Levoy and J. B. Vendersande, J. Met. 39 (1987), p.33

29] S. M. L. Sastry and J. E. O'Neal, as 9, p. 79.

30] P. Lovise Makin and Brian Ralph, J. Mater. Sci., 19 (1984), 3835.

31] C. Sigli and J. M. Sanchez, Acta Metall., 34 (1986), 1021.

32] A. J. McAlister, Bull. Alloy Phase Diagrams, 3(2), (1982), 177.

33] W.R.D. Jones and P.P.Das, J. Inst. Met, 87(1958-59), 338

34] Williams D.B., and Edington J.W., Met. Sci. J., Vol. 5, 1975, pp. 529-532.

35] Williams D.B., Al-Li Conf. V., Univ. Of Virginia, May 1989, pp. 551-563.

36] R. C. Dorward, Met. Trans. 19A, June 1988.

37] The Statistician, by Quant Systems, Charleston, SC, 1981.

38] S. Ranganathan and Alok Singh, Proc. of the seminar on science and tech. of Al-Li alloys., Bangalore, pp 37

39] Nozato R., and Nakai G., Trans. J.I.M., Vol. 18, 1977, pp. 679-689

40] A. K. Mukhopadhyay, C. N. J. Tite, H. M. Flower, P. J. Gregson and F. Sale, See 22, p. 439.

41] Papazian J. M., Sigli C., and Sanchez J.M., Scripta Met., Vol. 20, 1986, pp.201-206.

42] S. Ceresara, A. Giarada, and A. Sanchez, Philos. Mag., 1977, Vol. 35, 97-110.

43] Livet A., and Bloch D., Scripta Metall., Vol. 10, 1985, pp. 1147-1151

44] Spooner S., Williams D. B., and Sung C.M., Aluminium-lithium III, Eds. C. Baker et al., The Inst. Of Metals, London, 1986, pp. 329-336.

45] Balmuth E.S., Scripta Met., Vol. 18, 1984, pp.301-306.

46] Janos Lendvai, Hans-Joachim Gudladt, Wilfried Wunderlich, and Volkmar Gerold, Z. Metallkde.,1989,pp.310-317.

47] P. J. Gregson and H. M. Flower, J. Mat. Sci. Letters, 3, 829 (1984).

48] P. J. Gregson, H. M. Flower, C. N. J. Tite and A. K. Mukhopadhyay, Mat. Sci. Tech., 2, 349, 1986.

49] Al-Li 5 / 721

50] S. Fuzikawa, M. Furukawa, M. Sakauchi and K. Hirano, See 22, pp. 365.

51] P. L. Makin and B. Ralph, J. Met. Sci., 19, 3835 (1984)

52] Venables D., Christodoulou L., and Pickens J.R., Scripta Met., Vol. 17, 1983, pp. 1263-1268.

53] D.B. Williams, see 23, pp 90-100.

54] R.J. Rioja, P.E. Bertz, R.R. Sawtell, W.H. Hunt, and E.A. Ludwiczak, Aluminium Alloys-Their Physical and Mechanical properties. Proc. Int. Conf. at Charlottsville VA, Ed. E. A. Starke and T. H. Sanders Pub. EMAS., 1986, Vol. 3, pp. 1781.

55] D.J. Lloyd ICSMA 7, Montreal, 1986, Ed. H.J. McQueen, J.P. Balion, J.I. Dickson, J.J. Jonas, and M. G. Akben Pub. Pergamon Press Vol. 3, (1986), pp. 1745

56] P. Sainfort and B. Dubost, as 22, pp. 321

57] P. Sainfort and B. Dubost, as 22, pp. 407.

58] G.J. Kulkarni, D. Banerjee, and T.R. Ramachandran, Bull. Mater. Sci., Vol. 12, 1989, pp. 325-340

59] E.S. Balmuth, Scripta Metall., 18, (1984), 301.

60] S.F. Baumann, and D. B. Williams, Acta. Met., 33, (1985) 1069

61] E. S. Dwarakadasa, V. Subramaniam, M. Suryaprakash, G. S. Krishnadas Nair, as 38, pp. 108.

62] H. M. Flower, P. J. Gregson, C. N. J. Tite and A. K. Mukhopadhyay, as 53, Vol. 2, p. 743

63] R. J. Sinko, T. Ahrens, G.J. Shiflet, E.A. Stark Jr., see 35, pp. 375-383.

64] Amol A. Gokhale, Vijay Singh, Deep Kumar, and C.R. Chakravorthy, as 38, pp. 136

65] T.H.Sanders, Jr., as 8, pp 63.

66] I.M. Lifshitz, and V.V. Slyozov, J. Phys. Chem. Solids, 19, 35 (1961)

67] C. Wagner, Z. Electrochem, 65, 581 (1961)

68] M. Ahmad, and T. Ericsson, Scripta Metall., Vol. 19, 1985, pp. 457-462

69] B. Noble, S. J. Harris and K. Dinsdale, Met. Sci., 16 (1982), 425.

70] L. Hautefeuille, R. Rahouadj, Y. Barbaux and M. Clavel, See 6, pp. C3-669.

71] Ken-ichi Hirano, Mater. Sci. Forum, Vol. 13/14, (1987), pp.215.

72] S.M.L. Sastry, and J. E. O'Neal, as 8, pp.79-90.

73] K.S. Raman, Scripta Metall., 1971, 5, 791

74] Xia Xiaoxin and J. W. Martin, as 22, pp. 433

75] Ozbilen, as 35, pp. 651.

76] P. D. Pitcher, Scripta Metall., 22 (1988), 1301.

77] A. Grey, as 22, pp. 891

78] O. Jensrud, as 35, pp.411-419.

79] A.K. Vasudevan, E.A. Ludwiczak, S.F. Baumann, R.D. Doherty, M.M. Kersker, Mat. Sci. Engg., 72, 1985, pp.L25-L30.

80] E.A. Stark Jr., J. of Metals, 1970, pp. 54-63.

81] E. Hornbogen, Proc. 4th Int. Conf. on Strength of Metals and Alloys, Vol. 2, pp. 555-559, Nancy, France, 1976.

82] J. C. Huang and A. J. Ardell, as 44, pp. 455

83] W.A. Cassada, G.J. Shiflet and E.A. Stark Jr., as 61, Vol. 2, p. 695

84] N.J. Owen, P. hd. thesis, The University of London, 1987.

85] A. Loiseau and G. Lapasset, as 22, pp 331.

86] T. Ahrens, and E.A. Stark Jr., as 35, pp. 385-396.

87] T. H. Sanders Jr., and E.A. Stark Jr., Acta. Metall., 30, 927, (1982).

88] B.P. Gu, J.H. Kulwicki, G.L. Liedl and T.H. Sanders, J. M.S.E., 70, 217, (1985)

89] T.H. Sanders Jr., E.A. Ludwiczac, and R.R. Sawtell, M.S.E., 43, 247, (1980).

90] D. Jensrud, and N. Ryum, MSE, 64, 229, (1984)

91] D. W. Pashley, M.H. Jacobs, and J. T. Vietz, Phil. Mag., 16, 51, (1967)

92] R. B. Nicholson, J. Inst. Metals, 95, 91, (1967)

93] E.A. Stark Jr., J. Inst. Metals, 54, Jan. 1970.

94] S.C. Jha, T.H. Sanders Jr., and M.A. Dayananda, Acta Metall., Vol. 35, pp. 473-482, 1987

95] W. Seith, Diffusion In Solids, p. 162, Springer , Berlin, (1955)

96] L. P. Costas, U.S. Atomic Energy Commission Report, DP-813 (1963)

97] Shakesheff, as 35, pp. 201.